UNIVERSIDAD DE GRANADA

Facultad de Ciencias

GRADO EN FÍSICA

TRABAJO FIN DE GRADO

Uso de electrodos recubiertos de multicapas poliméricas cargadas *layer-by-layer* para la obtención de energía limpia por gradiente de salinidad

Presentado por:
D. Pablo Canca López

Curso Académico 2019/2020

Abstract

In this Bachelor's Thesis Capmix techniques are studied in order to obtain clean energy due to salinity difference, what is usually known as *Blue Energy*. Changes in the electrical double layer of the pores of an activated carbon electrode submerged inside an ionic solution will be studied both theoretically and experimentally. The *Soft Electrode* technique will be studied in detail. Two electrodes, both covered by a polyelectrolyte layer of different electrical sign and submerged in an ionic solution experience a potential difference equal to the difference between their *Donnan Potentials* without the need of membranes. These results will be obtained both theoretically and experimentally as well, to later present a theoretical innovation, consisting on the superposition of different polymeric layers covering the electrodes, with the aim of increasing the net extracted energy. A simulation will be used to obtain these results.

Resumen

En este TFG se estudian las técnicas Capmix para la obtención de energía limpia por diferencia de salinidad, normalmente conocidas como *Energía Azul*. Se estudiarán los cambios en la doble capa eléctrica de los poros de un electrodo de carbono activado sumergido en una solución iónica a partir de un modelo teórico y de manera experimental. Se estudiará en detalle la técnica de *Soft Electrodes*. Dos electrodos recubiertos ambos por capas poliméricas cargadas de signo contrario sumergidos en una solución iónica experimentarán una diferencia de potencial igual a la diferencia entre sus *Potenciales Donnan* sin necesidad de utilizar membranas. Estos resultados se obtendrán también de manera teórica y experimental, para después presentar una novedad teórica que supondría la superposición de distintas capas poliméricas recubriendo el electrodo, aumentando la energía extraída. Se utilizará una simulación que permitirá obtener estos resultados.

Mi agradecimiento a Ángel y a Silvia, sin cuya ayuda y apoyo durante estos años nunca habríamos llegado a este trabajo.

Contents

1 Introduction

1.1 Motivation

The search for clean, renewable energy resources is a must in our present day world, as many existing sources are limited, close to extinguishing and strongly contaminant. Fig. 1 [1] shows the situation in Spain, as recently as December 2019. Over 60 % of the electrical energy sources installed in our country come from non-renewable sources, including mainly nuclear, carbon, and fuel power stations. Note that, in spite of climatic considerations in Spain (sun radiation received per year), solar energy is a very modest contribution, and that we obtain most of the clean energy from hydraulic and eolic resources (about 40 %). Note here that the energy used in transportation is not included; in that case we should add a very important contribution of petroleum sources, as Fig. 2 [2] demonstrates: transportation takes almost 85 % of the energy production associated to petroleum consumption. As observed, there is still room for improving.

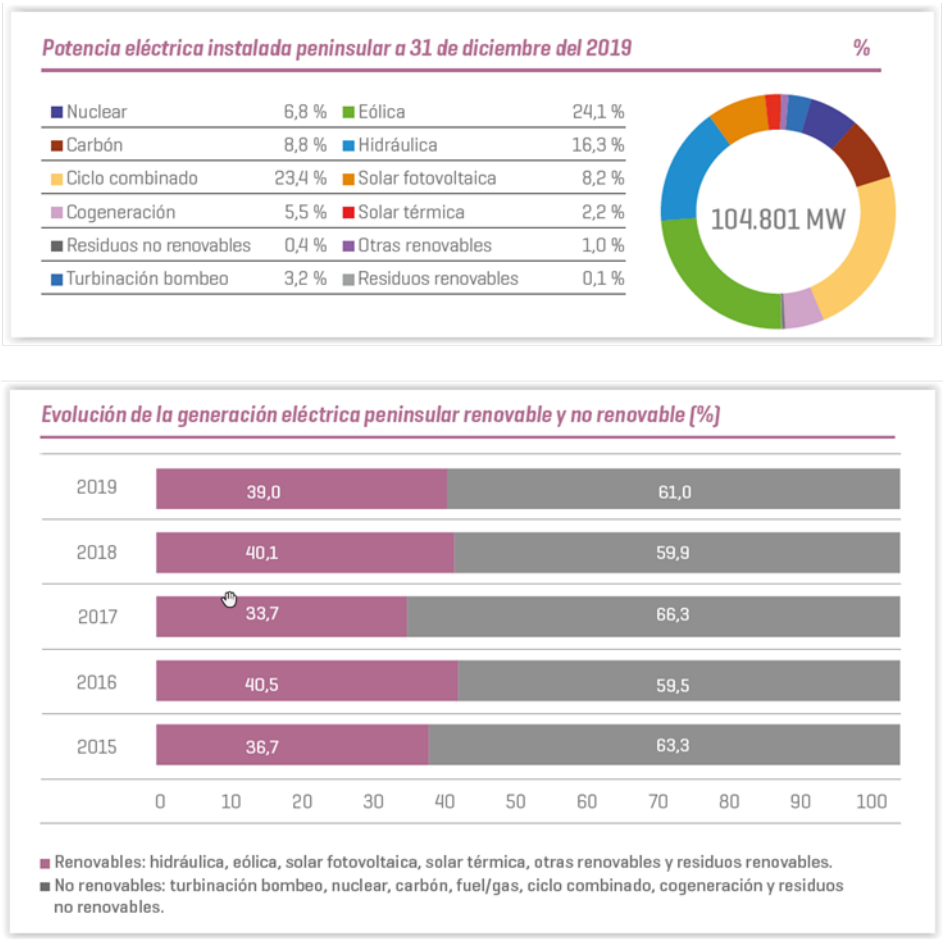

Figure 1: Energetic resources of peninsular Spain. Balance between renewable and non-renewable energies. Source: Red Eléctrica de España [1].

It is thus sufficiently justified to attempt even modest progress in new or improved clean energy sources. Although the leaders are obviously eolic, hydraulic and solar approaches, this does not mean exclusivity. The present project is a contribution to an addi-

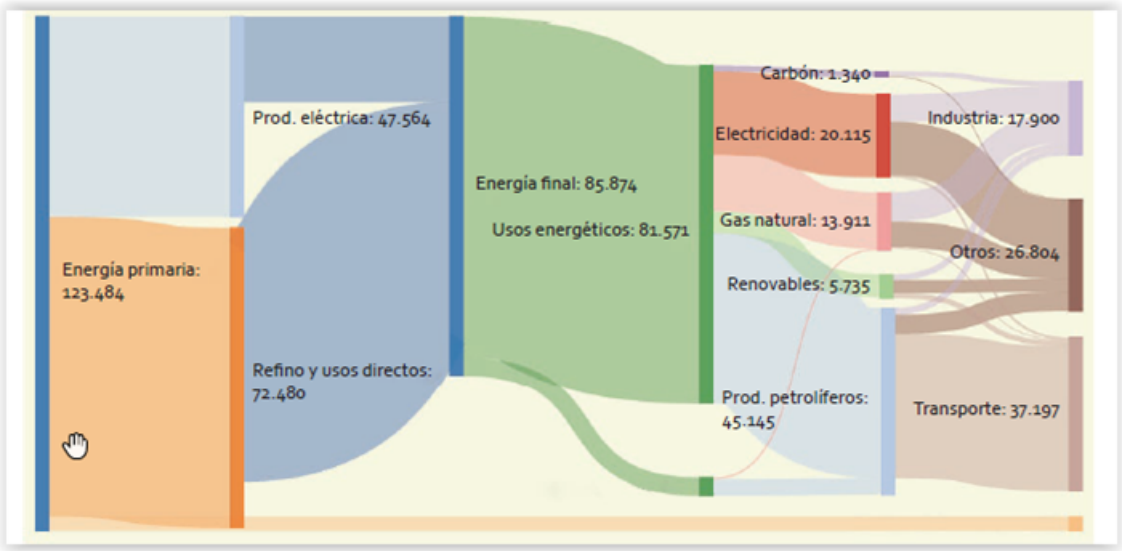

Figure 2: Energetic structure of Spain in 2016. Source: Ministerio de Energía, Turismo y Agenda Digital, Gobierno de España [2].

tional method, actually first proposed as early as 1954 by Pattle [3] (see also [4], and the detailed compilation provided in [5, 6]). It is currently known as *Salinity Gradient Energy Production* or *Blue Energy*, and it is based on the following facts.

Let us imagine that a volume V_f of fresh water with salt concentration c_f is mixed with a volume V_s of a concentrated solution containing c_s mol/V of salt. The resulting concentration of the mixture is c_{mix} (we could imagine a volume of river water mixing with sea in the river mouth). The free energy of the system would decrease (we assume constant temperature, so only the increase of entropy will count on the evaluation of free energy changes [6]):

$$\Delta G_{mix} = -2RT\left(V_f c_f \ln\frac{c_f}{c_{mix}} + V_c c_c \ln\frac{c_c}{c_{mix}}\right) \tag{1.1}$$

In the example of the river mouth, the volume of fresh (river) water is much smaller than that of the concentrated solution (sea water), and eq. (1.1) can be simplified to read:

$$\Delta G_{mix} = -2RTV_f\left(c_f \ln\frac{c_f}{c_c} + c_c\right) \underset{\left(V_f = 1\mathrm{m}^3,\, 300\ \mathrm{K}\right)}{\approx} 2\ \mathrm{MJ} \tag{1.2}$$

Quoting Norman [7]:

"The tremendous energy flux available in the natural salinations of fresh water is graphically illustrated if one imagines that every stream and river in the world is terminated at its mouth by a (silent) waterfall of 200 m."

1.2 Existing technologies for energy production by solution exchanging

Prior to presenting the chosen methods that will be studied in this Bachelor's Thesis (based on the electrical double layer expansion method) it is worth mentioning two very

important techniques that have reached a semi-industrial scale level. These are *Pressure-Retarded Osmosis* (PRO) and *Reverse Electrodialysis* (RED), both shown schematically in Fig. 3. The PRO technique considers the osmotic pressure difference between two water chambers separated by a membrane that is permeable only to the solvent (water). Fresh water diffuses into the salt-water container increasing the pressure in that chamber, up to 500 atm [8] for high salt concentration sea water. This accumulated pressure difference can be used to power a turbine, thus creating mechanical energy that can be converted into electrical energy. However, costs are high and they will remain so until more efficient and inexpensive membranes are developed [9].

RED takes a different approach, by using cation- and anion-exchange membranes. This will create a potential difference between two electrodes located on both sides of a cell. The water solution inside the cell is divided into different regions by intercalating membranes of alternate polarity. This technique was first developed by Pattle in the 1950s [10] and was further studied in the following years.

Finally, Capacitive Mixing (Capmix) methods take a more recent approach, based on the exchange of two solutions with different ion concentrations in a cell where two oppositely charged electrodes are located. Changes in the capacitance of the porous electrode/solution interface, together with the existence of a large specific surface area of contact (porous electrodes) are taken advantage of for producing voltage jumps between the electrodes, depending on the contacted solution. The first Capmix method to be developed, *Capacitive Energy Extraction by Double Layer Expansion* (or CDLE), was demonstrated by Brogioli in 2009 [11], and two other techniques would soon follow: CDP (*Capacitive Donnan Potential*, based on the use of membranes) [12], and SE (*soft* electrodes, utilizing polyelectrolyte-treated electrodes) [13]. The three of these will be further explained in the following chapters.

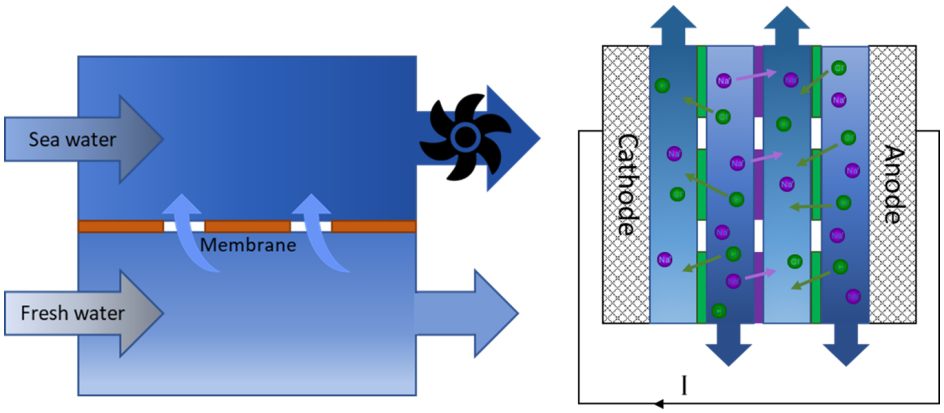

Figure 3: Schematics of PRO (left) and RED (right; green: anion-exchange membrane; purple; cation-exchange) methods.

1.3 The implementation of Capmix

A possible implementation has been carried out in our laboratory in recent years, inspired by the behavior of the ionic distribution around charged interfaces in contact with electrolyte solutions. The principles, to be detailed below, are as follows [11, 14, 15, 16, 17] (see Fig. 4). We will show that the ionic atmosphere (*Electrical Double Layer* or EDL)

surrounding a charged solid surface in contact with a solution containing free charges (ions) can adsorb a significant amount of ions, mostly counterions (i.e., those charged oppositely to the surface), from the solution. The two charged entities (surface and EDL) constitute a sort of capacitor, whose capacitance increases with the ionic content of the solution. Like in standard capacitors, increasing the capacitance (that is to say, increasing the ionic concentration) at constant charge brings about a reduction of the potential; this is a consequence of the increase of the EDL thickness, or, equivalently, of the plate-to-plate separation of the capacitor (*double layer expansion*). So, let us assume, as in Fig. 4, that the solid is conductive and it is connected to a battery in the presence of a high salt concentration (500 mM NaCl, sea water); this is point A in Fig. 4 (this corresponds to one of the electrodes; the other one will undergo identical processes, except for the charge and potential signs). The system is disconnected from the battery (the charge will remain constant if no leakage occurs), and the sea water is substituted by fresh or river water (30 mM, say). The potential of the EDL (the "capacitor") will increase. This is point B. The external circuit is subsequently discharged against an external load, until making again the potential difference between the electrodes equal to that of the external power source (point C). The following step is opening the circuit and letting salt water in, so that the potential is lowered (point D), and the system is ready for the last stage before starting over: charging by contacting with the battery. We note that after performing the cycle, electrical energy is obtained, as the system is charged externally (*energy input*) at lower potential than that in which it is discharged (*energy received*). This is the very basis of the so-called or CDLE, schematically presented in Fig. 4.

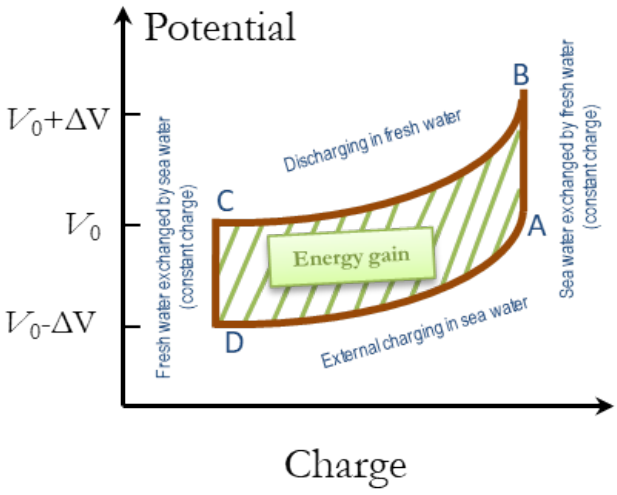

Figure 4: Schematics of the CDLE process. In A, the electrode is charged at the battery potential V_0, in presence of sea water. The potential raises to $V_0 + \Delta V$ when sea water is substituted by fresh water (point B). Discharging occurs in fresh water until reaching point C, and the same potential V_0. In D, salt water is again put into contact with the electrode, and the potential is lowered to $V_0 - \Delta V$. Finally, the system is charged again by contacting with the external power source.

1.4 Objectives and work plan

The main objectives of the work can be summarized as follows:

1. Review of the methods that have been proposed to obtain energy from salinity exchange.

2. Application to the case of so-called *soft electrodes*, that is, electrodes coated by a layer of polyelectrolyte.

3. Description of the model used for multiple-layer electrodes.

4. Describe the preliminary experiments carried out so far.

5. Discuss the predictions of the model, and, where possible, compare them with experimental data.

6. Analyze the future applicability of our method to *real-world* scale.

2 The Double Layer Expansion Method

2.1 The Electrical Double Layer

The structure of the solid/liquid interface in a ionic solution is well known and we will not provide an exhaustive description here, but rather a brief review of the basic concepts so that the reader can follow all our arguments. A detailed account can be found in the literature [18, 19, 20]. As mentioned before, when a solid surface is submerged in an ionic solution, ions with opposite charge to that of the surface (counterions) will be attracted to the solid, while those with the same charge (coions) will move in the opposite direction, thus leaving the solution in contact with an excess of countercharge, and providing electroneutrality. The charged surface and the compensating countercharges constitute the Electrical Double Layer. Even though it appears to be simple due to the word "double", its structure can be very complex, with several layers of ions. Without entering into unnecessary details, an informative scheme can be provided as in Fig. 5. Note that we can distinguish:

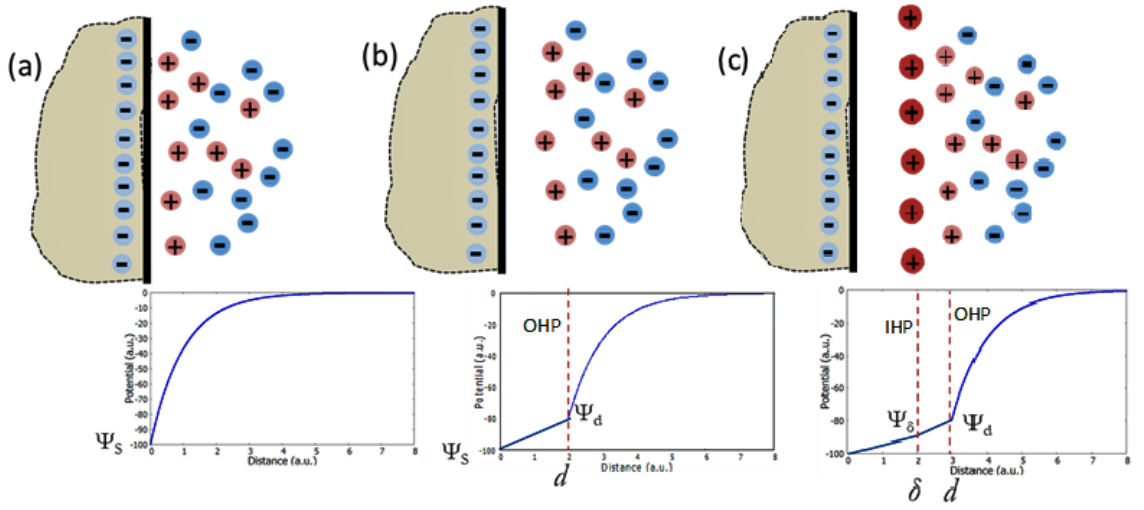

Figure 5: Schematics of EDL structure. (a): Gouy-Chapman; (b): Uncharged Stern layer; (c): Stern layer populated by specifically adsorbed ions.

1. *Gouy-Chapman* (GC) model*:* The charged surface, with charge density σ_s (although charges must be discretely spaced, we assume that for our macroscopic description it is reasonable substituting such discrete distribution by a homogeneous density). The potential on the surface (relative to a reference in the bulk of the solution, far from the interface) will be denoted by Ψ_s, the *surface* potential (Fig. 5 (a)). The charged diffuse layer begins right on this surface.

2. In a realistic description of the solution, ions cannot be considered point-like, but with a certain volume. This means that there is maximum approach distance of ions to the surface, which we call d. An ideal surface, called the *Outer Helmholtz Plane*, OHP, can be located on that position, and it marks the beginning of the diffuse part. The electric potential at this point is known as the *diffuse* or *Stern* potential, Ψ_d. A linear potential decay can be expected from the surface to the OHP. Note that the denomination *diffuse* is due to the fact that the countercharges do not stay on a real surface, but are extended somewhat into the bulk, as ions are influenced by both the local electrostatic field and diffusion forces, and the solvent will only be taken into account for its macroscopic dielectric permitivity (Fig. 5(b)). This description is known as Stern model of the EDL.

3. A still more complicated view is that there can be ions strongly attached to the surface (for instance, by chemical bonding mechanisms). These are not subject to diffusion and can even be charged with the same sign as the surface. By taking these considerations we speak of the Gouy-Chapman-Stern-Grahame description. The ideal charged surface associated to these (sometimes called *specifically adsorbed*) ions is denominated *Inner Helmholtz Plane* and it is located at a distance δ from the surface. The potential value is Ψ_δ (Fig. 5 (c)).

For the purposes of the present work, we will focus only on the diffuse part of the EDL, and later will consider the Stern approach. Once the beginning of the diffuse layer - beyond which the potential decays to zero - has been established, the potential $\Psi(\mathbf{r})$ can be calculated with the Poisson equation:

$$\varepsilon_0 \varepsilon_r \nabla^2 \Psi(\mathbf{r}) = -\rho(\mathbf{r}) = -\sum_{i=1}^{N} z_i c_i(\mathbf{r}) e \tag{2.1}$$

where $\rho(\mathbf{r})$ is the volume charge density at position $\mathbf{r}$, e is the charge of the electron, z_i is the valence of the *i-th* ionic species present in the solution and c_i its number concentration. This is obtained from the balance between electrostatic interactions with the solid and diffusive forces tending to oppose the counterion (coion) accumulation (depletion), leading to the Boltzmann equation ([21][22]):

$$c_i(\mathbf{r}) = c_{i0} \exp\left[-\frac{z_i e \Psi(\mathbf{r})}{k_B T}\right] \tag{2.2}$$

where c_{i0} is the concentration value far from the interface, k_B is the Boltzmann constant and T is the absolute temperature.

Substituting eq. (2.2) in eq. (2.1) the Poisson-Boltzmann equation is obtained:

$$\varepsilon_0 \varepsilon_r \nabla^2 \Psi(\mathbf{r}) = -\sum_{i=1}^{N} z_i e c_{i0} \exp\left[-\frac{z_i e \Psi(\mathbf{r})}{k_B T}\right] \tag{2.3}$$

In order to get a qualitative picture of the EDL structure, let us assume for the moment that the surface potential (hence, the potential at any position) is smaller that the *thermal potential* ($|\Psi| < k_B T/e$), so that the exponential can be expanded up to a first order in the potential, in what is known as the Debye-Hückel model:

$$\exp\left[-\frac{z_i e \Psi(\mathbf{r})}{k_B T}\right] \simeq 1 - \frac{z_i e \Psi(\mathbf{r})}{k_B T} \tag{2.4}$$

Substituting in eq. (2.3) and applying the electroneutrality condition $\left(\sum_{i=1}^{N} z_i e c_{i0} = 0\right)$, one has:

$$\nabla^2 \Psi = \sum_{i=1}^{N} \frac{z_i^2 e^2 c_{i0}}{k_B T \varepsilon_0 \varepsilon_r} \Psi = \kappa^2 \Psi \tag{2.5}$$

where κ (units $1/\mathrm{m}$) has a special significance. Indeed, if its assumed that the interface is planar, and that x is its perpendicular distance, then eq. (2.5) can be easily solved, leading to an exponential decay of the potential with distance, taking as boundary conditions $\Psi(x = d) = \Psi_d$, with d being the beginning of the diffuse layer, and $\Psi(x \to \infty) = 0$

$$\Psi(x) = \Psi_d e^{-\kappa x} \tag{2.6}$$

This shows that κ, called the *Debye-Hückel parameter*, is the inverse of the distance at which the potential decays $1/e$ in the diffuse layer. We can thus interpret κ^{-1}, also called the *Debye length*, as a measure of the *thickness* of the double layer. It is given by:

$$\kappa^{-1} = \sqrt{\frac{k_B T \varepsilon_0 \varepsilon_r}{\sum_{i=1}^{2} z_i^2 e^2 c_{i0}}} \tag{2.7}$$

Note that it depends inversely on the *ionic strength* or ionic content of the solution: the more concentrated the solution is, the thinner the EDL. This is illustrated in Fig. 6,

where equation (2.6) is solved for the case of two solutions with 30 and 500 mM NaCl and Ψ_d=100 mV. The effect of changing the sodium chloride concentration is clear: the EDL *capacitor* reduces significantly its plate-to-plate distance in presence of sea water.

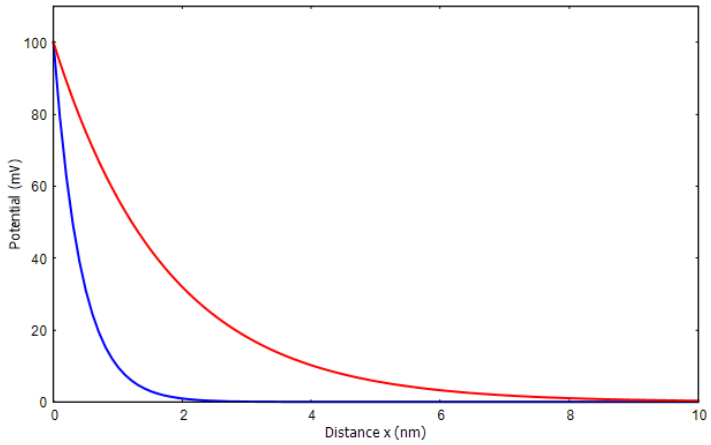

Figure 6: Potential vs. distance for a flat EDL with 100 mV surface potential, and the indicated NaCl concentrations.

Using the Boltzmann equation, eq. (2.2), it is possible to obtain the concentration profile, by simple substitution of the potential vs. distance dependence. An illustrative example is provided in Fig. 7 for the cases considered in Fig. 6.

Considering that the electrode materials are highly porous, it would seem that a better illustration can be obtained if cylindrical geometry is assumed for the EDL. The Poisson-Boltzmann equation will now read (laplacian operator in cylindrical coordinates):

$$\frac{d^2\Psi}{dr^2} + \frac{1}{r}\frac{d\Psi}{dr} = -\frac{1}{\varepsilon_r \varepsilon_0}\sum_{i=1}^{N} z_i e c_{i0} \exp\left[-\frac{z_i e \Psi}{k_B T}\right] \tag{2.8}$$

which must be numerically solved, although some semianalytical approximations have been proposed [23, 6]. As shown in Fig. 8, the general trends of the potential vs. distance to the wall dependencies are similar to those found for planar interfaces (Fig. 6), so the same qualitative arguments above discussed regarding EDL thickness are still applicable.

2.2 Energy extraction

The illustration shown in Fig. 7 of the EDL behavior when the ionic concentrations are changed gives us the necessary clues for understanding the process of energy extraction from the EDL compression and expansion sequences illustrated in Fig. 4. Let us imagine one porous electrode that has been charged for a very long time at a certain potential Ψ_0 while submerged in salty water (500 mM ionic concentration). Once fully charged, salty water is replaced by fresh water (20 mM) under open circuit conditions, allowing the accumulated charge to remain constant. At the same time, according to Eq. (2.7), the EDL becomes thicker, its capacitance increases, and so the voltage across the EDL increases. For a more clear understanding, it is possible to compare this with a classical capacitor, where the manual increase of the distance between the plates results, at a constant charge,

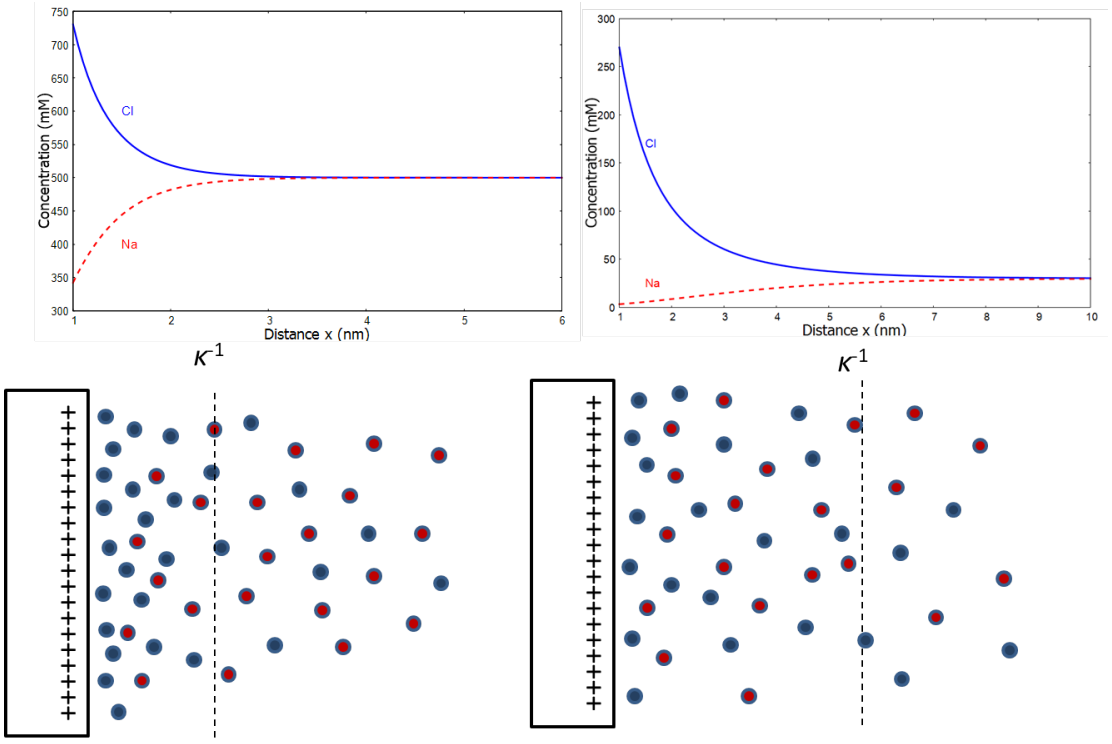

Figure 7: Variation of the ion concentration on the EDL, from a higher one (left) to a smaller one (right).

in a voltage increase ($C = \frac{Q}{\Delta V} = \frac{\varepsilon A}{d}$). Every pore will act as a capacitor, with the "manual" force being replaced by a diffusion force. We now imagine that two porous counter electrodes are placed in our cell, and charged with opposite voltages while in contact with a flowing ionic solution, for instance a salty one. We can control the process of opening or closing the circuit and of the pumps feeding the cell. The load resistors during the closed-circuit steps can also be changed if necessary (Fig. 9). Repeated four-step cycles will be performed, as represented in Fig. 10:

1. Both electrodes are oppositely charged by an external potential Ψ_0 with salty water between them.

2. The circuit is opened, allowing charge to remain constant. Fresh water replaces salty water, expanding the EDL. The electrode surface potential increases (by $\Delta\Psi$), since the capacitance decreases at constant surface charge.

3. The circuit is closed. The potential of the cell is higher than of the external source ($\Psi_0 + \Delta\Psi$), and thus the excess can be discharged through the load resistance R_{fresh}.

4. Salty water is allowed in again with open circuit, decreasing the voltage below Ψ_0 because of the same reason that made it increase in step 2.

Since a charge Q is given to the cell at a potential Ψ_0 and returned at a potential $\Psi_0 + \Delta\Psi$, $Q\Delta\Psi$ will represent the energy gain of the cycle. However, since an energy input is necessary for charging the cell, the area of the cycle (or area under step 4 minus under step 2) represents the net energy balance:

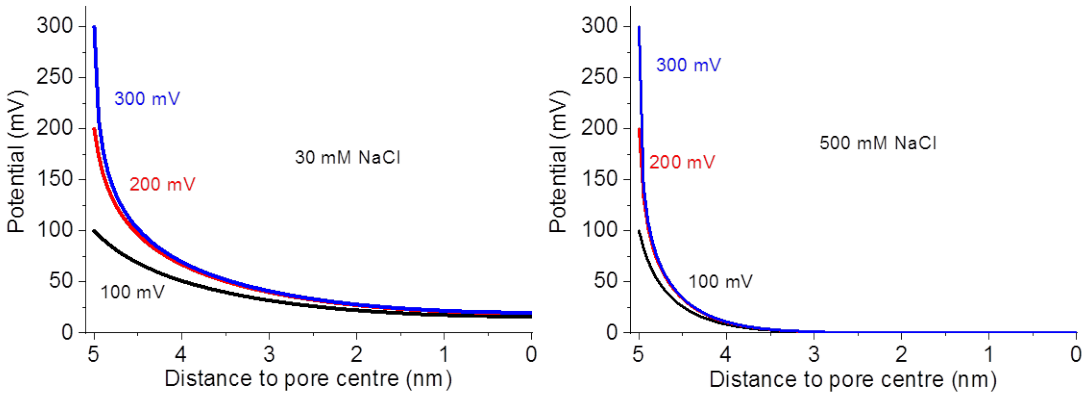

Figure 8: Potential vs. distance to the pore center for a cylindrical pore 5 nm in radius. Calculations performed for different wall potentials and two NaCl concentrations (Modified from Ref. [6]).

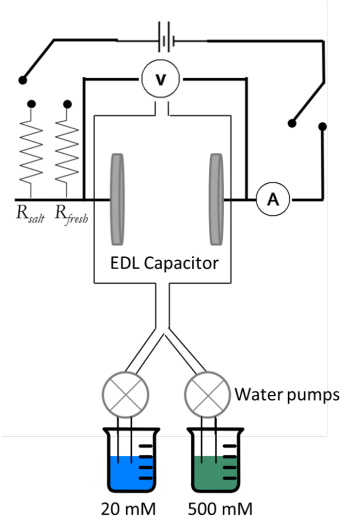

Figure 9: The CDLE implementation shown schematically.

$$E = -\int_{\sigma_{min}}^{\sigma_{max}} \left[\Psi_{Fresh} - \Psi_{Salty}\right] d\sigma \tag{2.9}$$

Because of charge leakage, it may happen that the recovered energy E is less than the energy used for charging. This is obviously an undesired situation that constitutes a serious drawback of the CDLE method, and that can only be overcome after careful selection of materials and procedures [5].

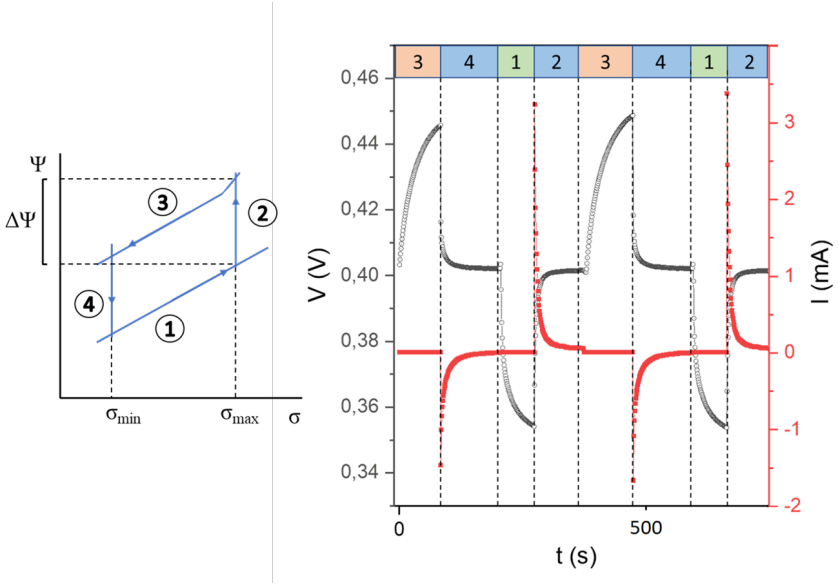

Figure 10: Illustration of the CDLE extraction process. Left: potential vs. charge; right: potential and current as a function of time.

3 Using membranes: Capacitive Energy Extraction by Donnan Potential (CDP)

Up to this point, an even distribution of ions across the two layers of the capacitor has been considered, obtaining a unbalanced distribution only after an external potential difference is applied. A method was proposed that allowed to perform cycles without the need of an external power source, and hence without the problem of energy losses [12, 24]. The method is denominated *Capacitive energy extraction by Donnan Potential* (CDP). As illustrated in Fig. 12, each electrode is now covered by a ion exchange membrane, one is a cation exchange (it contains negatively charged groups, that is, it is an *anionic membrane*), and the other exchanges anions (thus having positively charged groups, i.e., a *cationic membrane*). If one of these membranes, with a high concentration of (negative, say) charged groups, is placed in a bath with a certain concentration of ions, it will attract cations until an electric field is established that opposes their absorption. A negative potential difference will exist between the interior of the membrane and the bulk of the solution. This is the *Donnan potential*. It will be positive for a negatively charged membrane, and it will increase in absolute value when the salt concentration decreases (Fig. 11). If the concentrations on both sides of the membrane are different, the Donnan potentials will be different on each side, and a membrane potential is thus generated. This will give rise to a potential difference without any external power needed -a sort of self-sufficient method. Without an external source, leakage becomes a secondary problem, thus obtaining better results than with CDLE [12][25].

Energy is obtained by changing the solutions that flow between the electrodes (fresh or salty), leading to an increase of the Donnan Potential for the case of fresh water and a decrease for salty water. An external resistance will allow the current to flow through, thus obtaining energy. The schematics of the implementation of a CDP cycle are shown in Fig. 12.

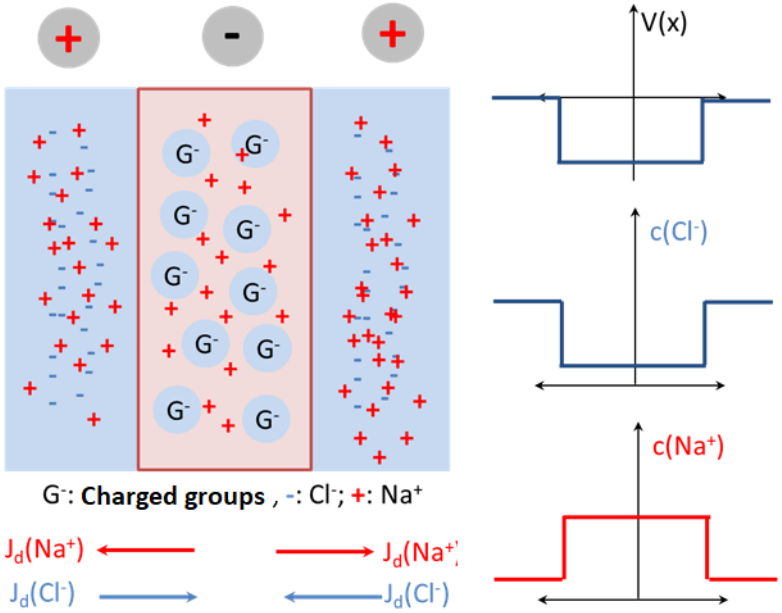

Figure 11: Generation of the Donnan potential for a highly charged membrane submerged in an ionic solution. The concentration of ions is the same on both sides.

Two electrodes are submerged in fresh water (a), allowing cations and anions to pass through the cationic (left) and anionic (right) membranes respectively. There is a potential inside the membrane since the charge on the side of the electrode is zero for both cases, and it's different from zero on the solution side. Now salt water is allowed in under open circuit conditions (b), thus reducing the potential difference between both sides of the membrane since ions are located now inside the pores of the electrodes. However, a potential difference between both electrodes now appears because of the charge difference, and a big potential jump can be seen inside each electrode, positive for the one on the right and negative on the left one. If the circuit is closed (c) charge will be redistributed until the potential drops back to zero between the electrodes (d). Fresh water is allowed in again (e) hence ions will move from the electrode to the solution because of diffusion. The potential difference between each electrode and the solution will be much bigger now because of the charge difference between the two mediums. The potential inside the electrode will thus change to compensate for this, since we are working under open circuit conditions. Finally, the circuit is closed (f), giving rise to a current I that will last until both electrodes have no potential difference, thus returning to stage (a).

4 The case of Soft Electrodes

It is worth mentioning a big challenge of the CDP method: membranes are expensive and prone to scaling, and additionally they can release chemicals into the water [26], thus impacting (moderately in fact) the environment. In an attempt to preserve the advantages while minimizing drawbacks, Ahualli et al. [13] invented a modification in which, instead of using membranes, the carbon electrodes were coated with a layer of polyelectrolyte (cationic and anionic, respectively). Because this layer is permeable to counterions

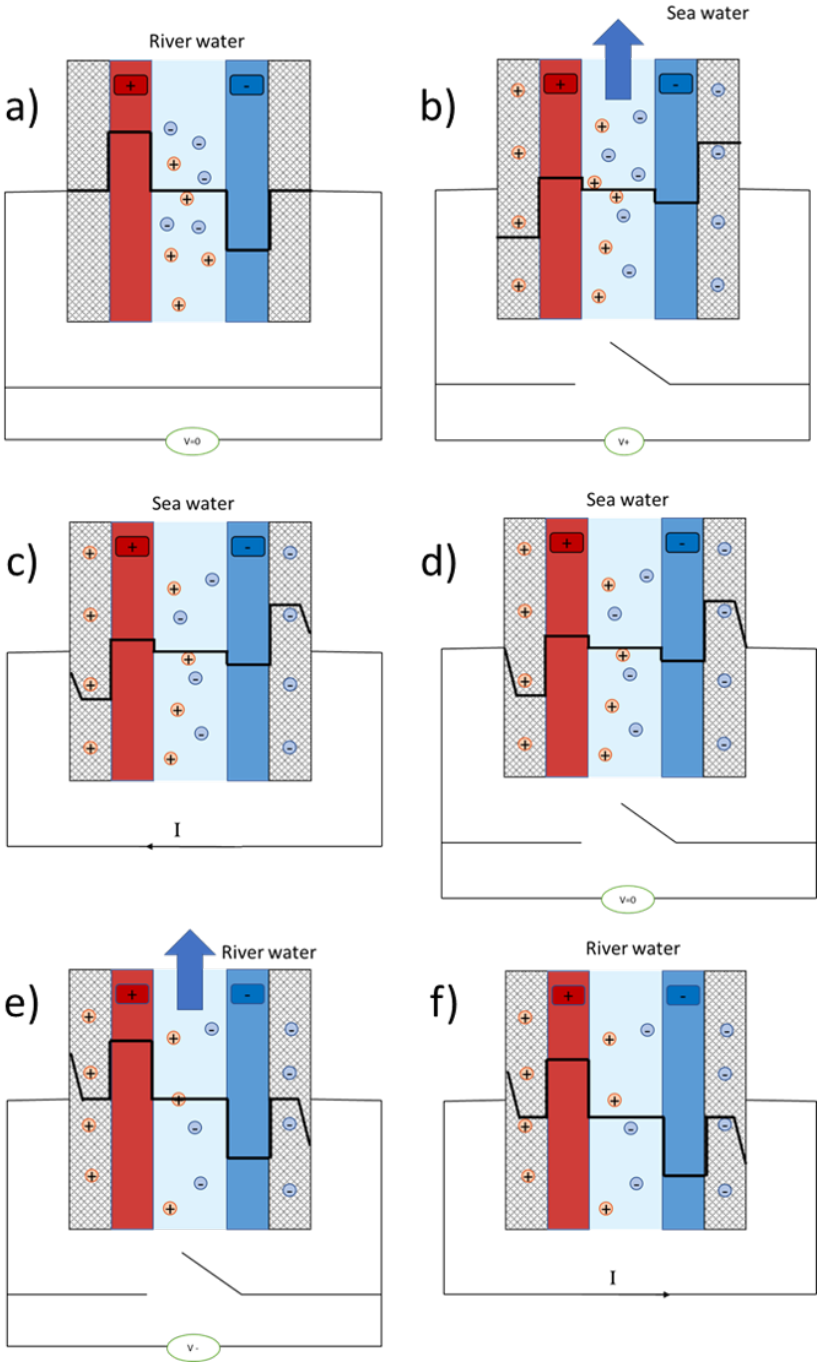

Figure 12: Schematics of a CDP cycle and potential profile. a) Both electrodes have been submerged in fresh water for a period of time. The anionic membrane allows anions to pass through, the cationic one allows cations in. b) The circuit is opened and salty water runs between the electrodes. More ions make it through the membrane because of diffusion c) Because a potential difference appears, current will flow between the electrodes until it drops to zero. d) The circuit is opened once the potential between the electrodes is zero. e) Fresh water is allowed in, thus creating a potential difference, negative this time. Ions make it out of the membrane, back into the solution, because of diffusion. f) The circuit is closed again, giving rise to a current I. Stage a) would follow next.

and solvent, the technique was denominated *soft electrode* (SE) method. The name comes from the one given to nanoparticles coated by charged macromolecules (soft particles), also widely studied in the group [27, 28]. The soft electrode technique combines two approaches: the CDLE, based on the expansion of the EDL, and the Donnan potential method, the CDP, as will be explained below.

4.1 The SE method

As mentioned, soft electrodes consist of an activated rigid carbon core coated with a polyelectrolyte layer (a soft, solvent-permeable, highly charged layer [13]), which can be cationic or anionic. This polyelectrolyte layer will be thick enough to give rise to a Donnan Potential on each electrode, without the need of membranes, when submerged in an ionic solution. We assume that both electrodes will be coated by symmetrical polyelectrolyte layers, differing only in sign, for a simpler discussion. Similarly to the CDP method, no external power supply is required, but the potential difference in the cell will be, as in the CDLE method, due to processes happening on the pores. The energy gain will be then given by both the Donnan Potential and the expansion of the EDL.

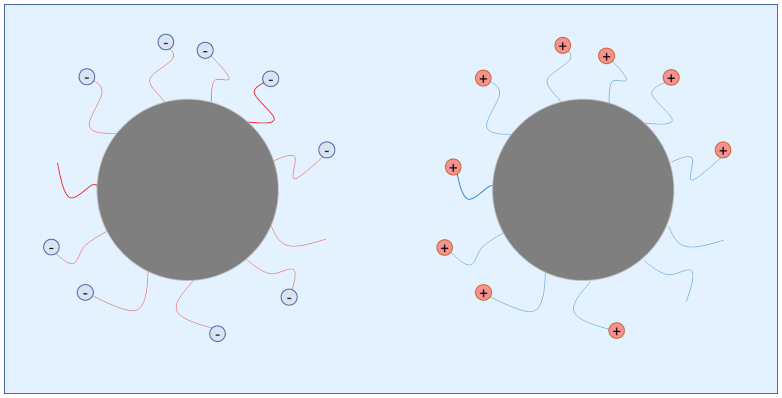

Figure 13: Representation of two carbon surfaces coated by a cationic polyelectrolyte layer (left) and an anionic one (right) submerged in an ionic solution. Both are represented in gray since they have not yet accumulated charge.

In order to obtain the potential and charge distributions in the system, the electric potential Ψ can be calculated once again through the Poisson equation

$$\varepsilon\varepsilon_0\nabla^2\Psi = -\rho(\mathbf{r}) \tag{4.1}$$

but in this case it must be split into three different regions: inside the rigid core, inside the polyelectrolyte layer (of radius R_{pol}) and beyond.

$$\varepsilon_r\varepsilon_0\nabla^2\Psi = \begin{cases} 0 & r < R_{\text{core}} \\ -\rho_{\text{sol}}(\mathbf{r}) - \rho_{\text{pol}}(\mathbf{r}) & R_{\text{core}} < r < R_{\text{pol}} \\ -\rho_{\text{sol}}(\mathbf{r}) & R_{\text{pol}} < r \end{cases} \tag{4.2}$$

where $\rho_{\text{sol}}(\mathbf{r}) = \sum_{i=1}^{N} z_i c_i e$ just as in equation (2.1) and $\rho_{\text{pol}}(\mathbf{r})$ is the charge density of the polyelectrolyte layer. We take the charge density inside the core to be zero, for

charge is all located on its surface, and the polyelectrolyte to be permeable to the solution. Outside this layer, just like in section 2.1, the charge density comes from the distribution of ions in the solution.

In order to solve these equations, which will be done in following chapters, spherical symmetry will be assumed. The boundary conditions will then be:

$$\left.\frac{\mathrm{d}\Psi}{\mathrm{d}r}\right|_{r=R_{\mathrm{core}}} = \frac{-\sigma}{\varepsilon_r \varepsilon_0} \tag{4.3}$$

$$\left.\frac{\mathrm{d}\Psi}{\mathrm{d}r}\right|_{r\to\infty} = 0 \tag{4.4}$$

Continuity between the regions must be satisfied:

$$\Psi(r = R^+_{\mathrm{pol}}) = \Psi(r = R^-_{\mathrm{pol}}) \tag{4.5}$$

$$\left.\frac{\mathrm{d}\Psi}{\mathrm{d}r}\right|_{r=R^+_{\mathrm{pol}}} = \left.\frac{\mathrm{d}\Psi}{\mathrm{d}r}\right|_{r=R^-_{\mathrm{pol}}} \tag{4.6}$$

with the $\pm$ signs representing the inner/outer sides of the region.

It is possible to solve these differential equations numerically using spherical pores:

$$\frac{d^2\Psi}{dr^2} + \frac{2}{r}\frac{d\Psi}{dr} = \begin{cases} 0 & r < R_{\mathrm{core}} \\ -\frac{1}{\varepsilon_r\varepsilon_0}\sum_{i=1}^{N} z_i e c_{i0} \exp\left[-\frac{z_i e \Psi}{k_B T}\right] - \frac{\rho_{\mathrm{pol}}}{\varepsilon_r\varepsilon_0} & R_{\mathrm{core}} < r < R_{\mathrm{pol}} \\ -\frac{1}{\varepsilon_r\varepsilon_0}\sum_{i=1}^{N} z_i e c_{i0} \exp\left[-\frac{z_i e \Psi}{k_B T}\right] & R_{\mathrm{pol}} < r \end{cases} \tag{4.7}$$

A Matlab routine was written to solve the equations. Fig. 14 illustrates the results for two different NaCl concentrations. Note the approximate constancy of the potential inside the polymer layer (Donnan potential), and how this constant value is larger in more diluted NaCl solutions.

A complete cycle would go as follows (Figs. 15):

1. Uncharged coated cores are submerged in salty water. Donnan potentials are established. There is no EDL potential, since the particles are not charged, thus the surface potential of each electrode will match the Donnan potential. The potential difference between both electrodes V will then be twice the Donnan Potential (Fig. 15a).

2. Both electrodes are externally connected, transferring charge from one to another (in this case, from left to right) and thus forming EDLs close to the surfaces. There is a superposition of both potentials -Donnan and EDL- in this region and, being of opposite signs, a drop of the overall absolute value of the potential will appear. Eventually, both electrodes will become equipotential (both zero, because of the polyelectrolyte layers symmetry) and charge transfer will stop (Fig. 15b).

3. Fresh water is allowed in and the external circuit is disconnected, thus creating a rise in the absolute value of both Donnan potentials (because of the lower concentration) and of both EDL potentials (because of the double layer expansion at fixed charge

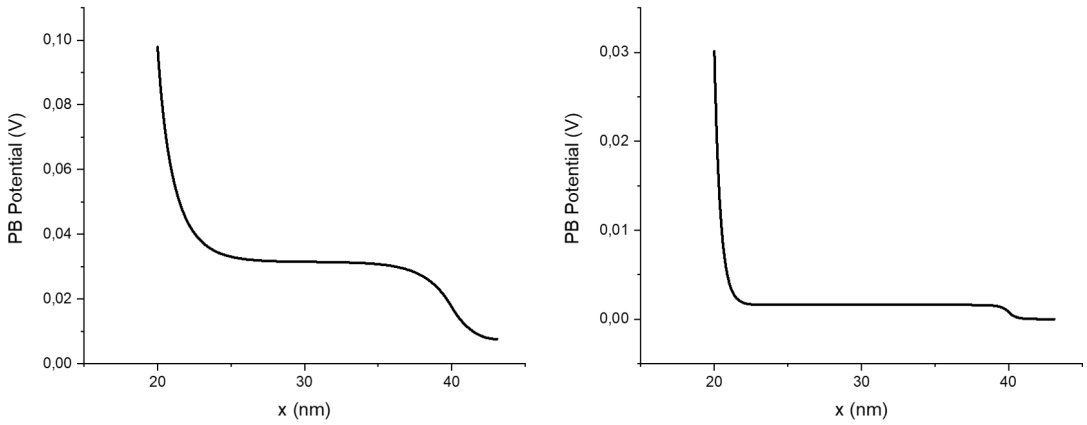

Figure 14: Potential profile for a core of radius 20 nm covered by a polyelectrolyte coating of radius 30 nm and charge density $\rho_{pol} = 6 \times 10^6\,\mathrm{C/m^3}$, σ_S=0.05 $\mathrm{C/m^2}$. Calculations performed for NaCl concentrations of 20 mM (left) and 500 mM (right)

on the surface). Since the weight of the Donnan potential increase is bigger, this results in a net increase of both surface potentials (Fig. 15c).

4. Both electrodes are again reconnected, leading to a charge flow towards the right electrode until equipotentiality is restored. The potential at the surface will be zero once again because of the symmetry of the system (Fig. 15d).

5. Finally, the circuit is opened once again and fresh water is replaced by salty water (Fig. 15e). Closing the circuit again will redistribute the charge towards the left, bringing us back to step 2 (Fig. 15f).

This process, although similar to CDP, differs in the origin of the potential difference. In CDP, a surface potential appears as a consequence of the membrane potential, which is generated because of the salinity difference between two sides of a membrane. However, in the SE case the surface potential is directly the Donnan potential, since the polyelectrolyte layer is directly adjacent to the surface of the electrode. It is interesting to note again that there will always be a net energy gain, since there is no external voltage applied. As an example, Fig. 16 shows the typical dependencies between the charge transferred between the electrodes and the potential difference between them.

By connecting our coated electrodes to a resistance and changing the water they are submerged into, it is possible to obtain a figure of the potential against charge. A theoretical solution can be obtained by finding the surface charge density that makes V=0. There will be two surface charge densities that yield this solution, depending on whether we are working with salty water (step 2) or fresh water (step 4). Steps 3 and 5 are obtained by changing the water but not the surface charge density, as can be seen in Fig. 16.

4.2 Multilayer electrodes

A possible improvement of the SE method is presented here. In the previous case, nothing prevented the polyelectrolyte layer from detaching from the electrode but its own stick-

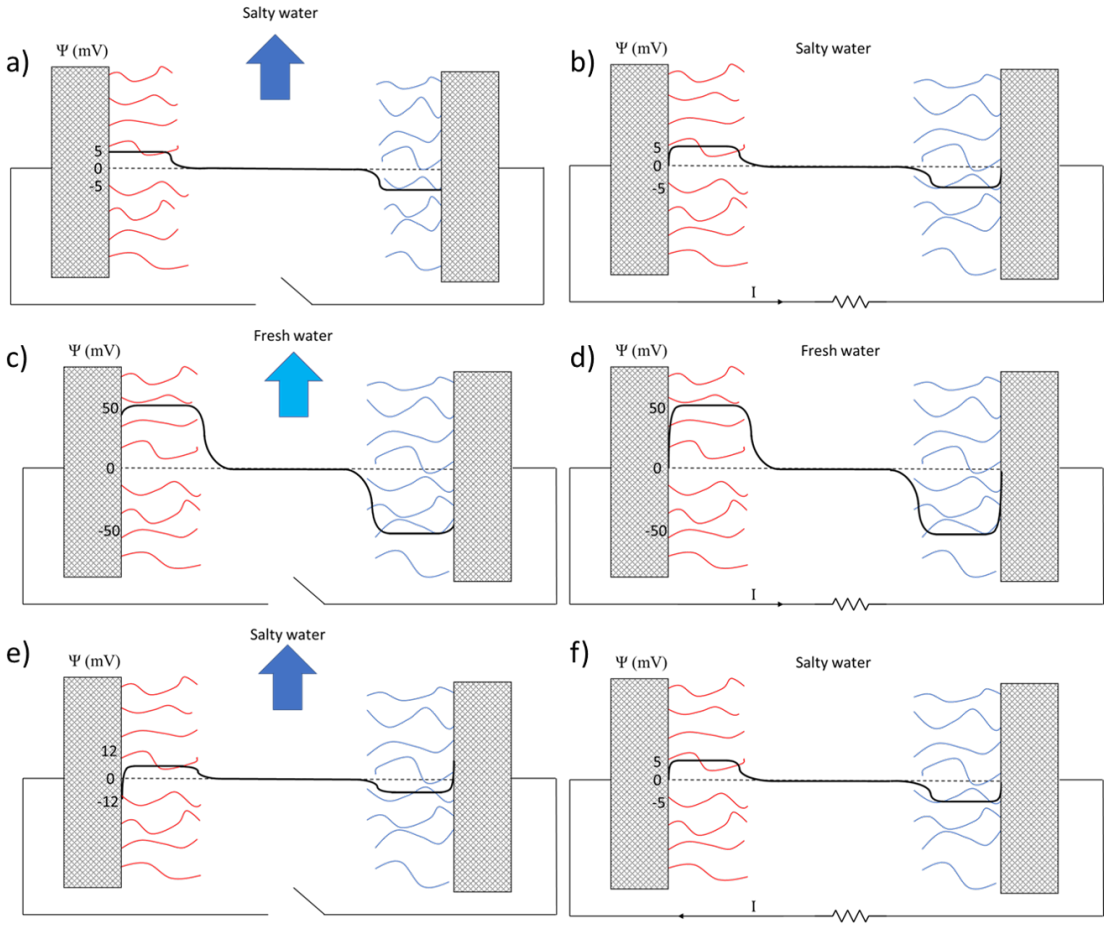

Figure 15: (a) Carbon electrodes (in Grey) are coated with a cationic polyelectrolyte (left, in red) and an anionic one (right, in blue). (b) Carbon electrodes are now externally connected, and become charged since a current I arises, transferring charge from left to right as the right electrode has a lower potential. (c) Fresh water is allowed in, at open circuit, and both potentials experience an increase in absolute value. Note that the scales are changed. (d) A current I moves charges from left to right as a result of the potential difference. (e) Salt water goes into the cell, the Donnan potential is lower, and the EDL is compressed. (f) When the circuit is closed again, a current I would appear, this time in the opposite direction since the potential was lower on the left electrode. (Modified from Ref. [6])

iness, thus not being a homogeneous, completely efficient layer. In order to increase its efficiency, more than one layer of polyelectrolyte can be added, having the fist layer, say, positive and the next one negative, thus increasing its stability. What we should achieve is a more firm structure that enhances the attachment between the electrodes and the first layer while keeping the potential difference the same, what will increase the adsorbance of ions of opposite charge to the last added layer.

By adding more layers, the Poisson-Boltzmann will be split into more regions:

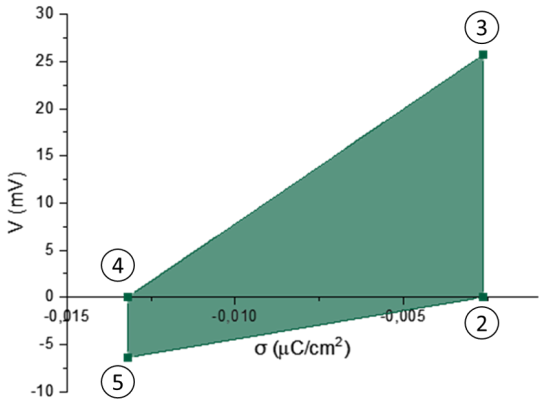

Figure 16: Theoretical voltage vs surface charge density for a carbon electrode. 20 mM and 500 mM waters are exchanged. Polyelectrolyte charge density of $6 \times 10^6\,\mathrm{C/m^3}$. Polyelectrolyte layer of radius $R = 30\,\mathrm{nm}$. Each number represents a step of the cycle as described in this chapter.

$$\frac{d^2\Psi}{dr^2} + \frac{2}{r}\frac{d\Psi}{dr} = \begin{cases} 0 & r < R_{\mathrm{core}} \\ -\frac{1}{\varepsilon_r\varepsilon_0}\sum_{i=1}^{N} z_i e c_{i0} \exp\left[-\frac{z_i e\Psi}{k_B T}\right] - \frac{\rho_{\mathrm{pol}1}}{\varepsilon_r\varepsilon_0} & R_{\mathrm{core}} < r < R_{\mathrm{pol}1} \\ -\frac{1}{\varepsilon_r\varepsilon_0}\sum_{i=1}^{N} z_i e c_{i0} \exp\left[-\frac{z_i e\Psi}{k_B T}\right] - \frac{\rho_{\mathrm{pol}2}}{\varepsilon_r\varepsilon_0} & R_{\mathrm{pol}1} < r < R_{\mathrm{pol}2} \\ -\frac{1}{\varepsilon_r\varepsilon_0}\sum_{i=1}^{N} z_i e c_{i0} \exp\left[-\frac{z_i e\Psi}{k_B T}\right] - \frac{\rho_{\mathrm{pol}3}}{\varepsilon_r\varepsilon_0} & R_{\mathrm{pol}2} < r < R_{\mathrm{pol}3} \\ \vdots & \vdots \\ -\frac{1}{\varepsilon_r\varepsilon_0}\sum_{i=1}^{N} z_i e c_{i0} \exp\left[-\frac{z_i e\Psi}{k_B T}\right] & R_{\mathrm{pol}N} < r \end{cases} \tag{4.8}$$

In this work, we will take the cases of one, two and three alternating polyelectrolyte layers.

The boundary conditions will then remain the same -two equations as in (4.3), (4.4)-, whereas, since this time there are be N+1 equations, there will be 2(N+1) continuity equations with the form

$$\Psi(r = R^{+}_{\mathrm{pol\,n}}) = \Psi(r = R^{-}_{\mathrm{pol\,n}}) \tag{4.9}$$

$$\left.\frac{\mathrm{d}\Psi}{\mathrm{d}r}\right|_{r=R^{+}_{\mathrm{pol\,n}}} = \left.\frac{\mathrm{d}\Psi}{\mathrm{d}r}\right|_{r=R^{-}_{\mathrm{pol\,n}}} \tag{4.10}$$

5 Theoretical predictions

5.1 Basic equations

Equations from chapter 4.1 can be solved by using a MatLab simulation. In order to implement the equations they must first be nondimensionalized. New parameters are thus defined as follows:

$$\alpha_i = \frac{z_i c_{i_0}}{\sum_{i=1}^{N} z_i^2 c_{i_0}} \tag{5.1}$$

$$x = \kappa r \tag{5.2}$$

For a spherical case, considering radial symmetry

$$h(r) = \frac{e}{k_B T}\Psi(r) \Longrightarrow \nabla^2 h(r) = \frac{k_B T}{e}\left[\frac{2}{r}\frac{dh}{dr} + \frac{d^2h}{dr^2}\right] \tag{5.3}$$

Therefore, it is possible to express $h(r)$ in terms of x and of a constant α_i, both nondimensionalized, for equation (4.2), in the outer region:

$$\frac{d^2h(x)}{dx^2} = -\frac{2}{x}\frac{dh(x)}{dx} - \sum_{i=1}^{N} \alpha_i e^{-z_i h(x)} \tag{5.4}$$

For the second region, inside the polyelectrolyte layer, we take the same approach and obtain

$$\frac{d^2h(x)}{dx^2} = -\frac{2}{x}\frac{dh(x)}{dx} - \sum_{i=1}^{N} \alpha_i e^{-z_i h(x)} - \frac{\rho_{pol} e}{k_B T \varepsilon_0 \varepsilon \kappa^2} \tag{5.5}$$

resulting in two nondimensionalized equations.

Boundary conditions must also be nondimensionalized, resulting in

$$\left.\frac{\mathrm{d}h}{\mathrm{d}x}\right|_{x=X_{\mathrm{core}}} = \frac{-e\sigma}{k_B T \varepsilon \varepsilon_0} \tag{5.6}$$

$$\left.\frac{\mathrm{d}h}{\mathrm{d}x}\right|_{x\to\infty} = 0 \tag{5.7}$$

where $X_{\mathrm{core}} = R_{\mathrm{core}}\kappa$. For the continuity conditions the same applies

$$h(x = X^{+}_{\mathrm{polyel}}) = h(x = X^{-}_{\mathrm{polyel}}) \tag{5.8}$$

$$\left.\frac{\mathrm{d}h}{\mathrm{d}x}\right|_{x=X^{+}_{\mathrm{polyel}}} = \left.\frac{\mathrm{d}h}{\mathrm{d}x}\right|_{x=X^{-}_{\mathrm{polyel}}} \tag{5.9}$$

It is then possible to solve equations (5.4) and (5.5). Furthermore, this can be done with as many polyelectrolyte layers as we want following the same procedure, thus being able to observe the changes in the potential as more layers are added.

5.2 Predictions

5.2.1 Single layer

For a single layer of thickness 10 nm with a charge density $\rho_{pol} = 6 \times 10^6\,\mathrm{C/m^3}$ it is possible to find the surface charge density variation by changing its value until the potential V becomes zero with salty water running through. This means we are at step 2 according to Fig. 16. By changing the water to fresh and moving the surface charge density forward, another zero is found, corresponding to step 4. Fig. 17 shows the result of the simulation.

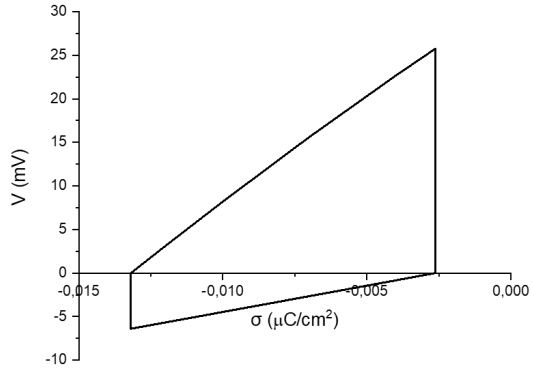

Figure 17: Theoretical voltage vs surface charge density for a carbon electrode. 20 mM and 500 mM waters are exchanged. Polyelectrolyte charge density of $6 \times 10^6\,\mathrm{C/m^3}$. Polyelectrolyte layer of thickness 10 nm.

The area of the inside region yields the energy density extracted from the cycle, resulting in $E = 0.17\,\mathrm{mJ/m^2}$.

We present in Fig. 18 the voltage profiles of one electrode for surface charge density $\sigma_S = 0$. On the left, the electrode is submerged in fresh water and, on the right, in salty water. Note the big rise of the Donnan Potential, going from 1.6×10^{-3} V to 0.03 V when fresh water is allowed in. This increase, of one order of magnitude, is due to a lower concentration of ions, as commented in previous sections. Note that the potential begins directly at its maximum, the Donnan Potential, and not at a smaller one. If the electrode were charged this would not be the case: the electrode's own potential and its EDL would have an effect on the potential profile, resulting on a small increase at first followed by a saturated region and then, finally, a progressive decrease once outside the polyelectrolyte layer. This can be seen schematically in Fig. 15c.

This same process has been simulated for a polyelectrolyte with charge density of $12 \times 10^6\,\mathrm{C/m^3}$. In Fig. 19 voltage vs surface charge density is represented. This time, an energy of $0.46\,\mathrm{mJ/m^2}$ is obtained, more than twice as much as before.

The same voltage profiles were obtained, thus they will not be shown again. The only difference lies on the Donnan Potential, which goes from 3.2×10^{-3} V for salty water to 0.047 V for fresh water, hence more energy is extracted.

The importance of the surface charge density - and hence, also of the thickness of the layer- and its relationship with energy extraction have been established. Were these

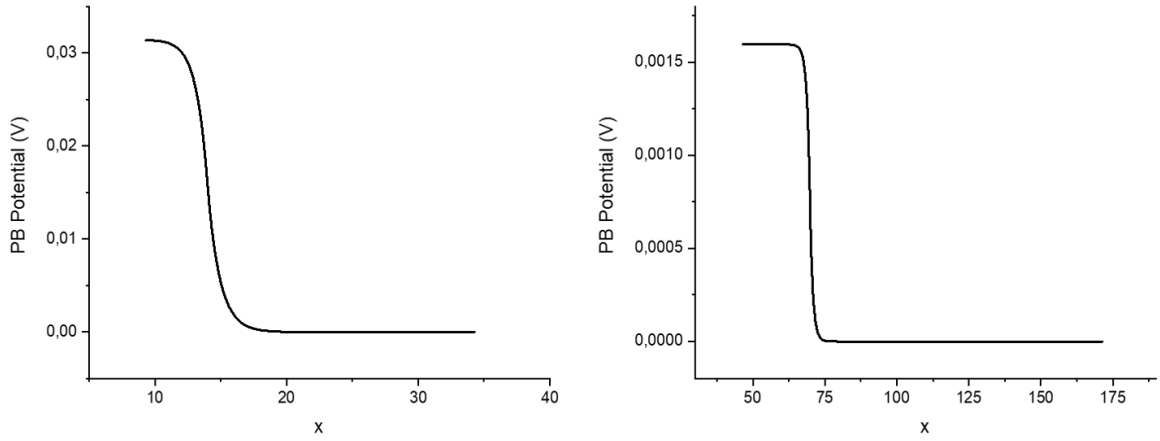

Figure 18: Voltage profiles obtained by solving the Poisson-Boltzmann equation for a porous electrode covered by one polyelectrolyte layer of charge density $6 \times 10^6\,\mathrm{C/m^3}$ and thickness 10 nm. Left: fresh water (20 mM), discharged electrode. Right: salty water (500 mM), discharged electrode.

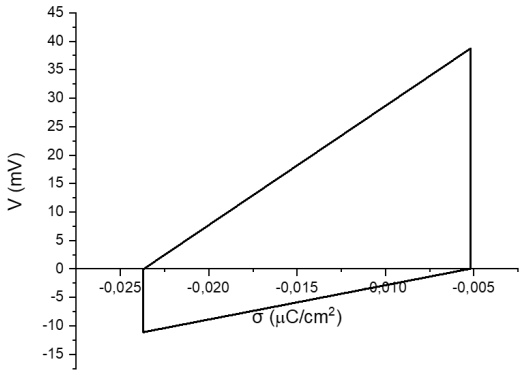

Figure 19: Theoretical voltage vs surface charge density for a carbon electrode. 20 mM and 500 mM waters are exchanged. Polyelectrolyte charge density of $12 \times 10^6\,\mathrm{C/m^3}$. Polyelectrolyte layer of thickness 10 nm.

experimental results, we would not obtain such thick, homogeneous layers. Instead, an irregular layer would stick to the electrode, with smaller average radius and lower charge density. A second layer of opposite sign would, theoretically, stick much better.

5.2.2 Two layers

Let us imagine first that both layers cover the electrode perfectly, both with a charge density of $6 \times 10^6\,\mathrm{C/m^3}$, only with a negative sign for the second one. The thicknesses are 10 nm for the first and second layers. This is shown in Fig. 20.

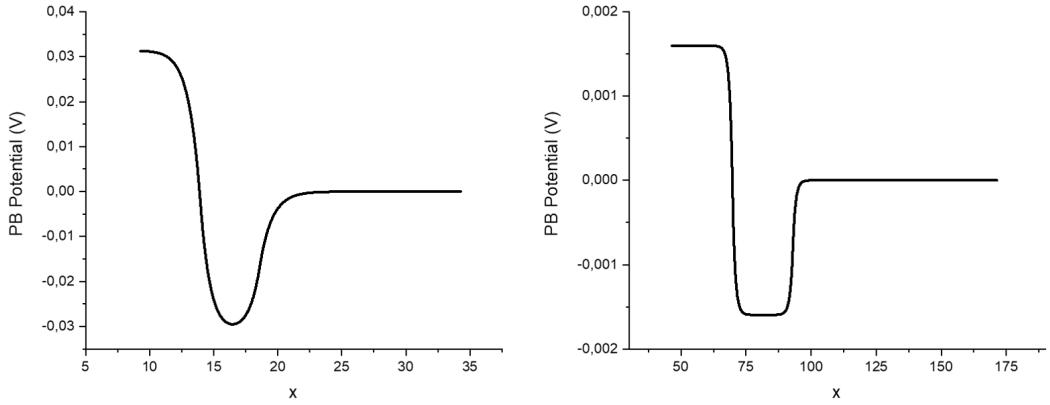

Figure 20: Voltage profiles obtained by solving the Poisson-Boltzmann equation for a porous electrode covered by two polyelectrolyte layers of charge densities $\rho_1 = 6 \times 10^6\,\mathrm{C/m^3}$, $\rho_2 = -6 \times 10^6\,\mathrm{C/m^3}$ and thicknesses 10 nm. Left: fresh water (20 mM), discharged electrode. Right: salty water (500 mM), discharged electrode.

The same Donnan Potentials are obtained, just as if we only had one polyelectrolyte layer. This shows the heavy influence of the first layer. However, this is an ideal case, something we would never obtain in a laboratory. Let us imagine an experience somewhat closer to reality, where the first polyelectrolyte layer has a much smaller average thickness, of 2 nm, and also a smaller charge density, of $0.5 \times 10^6\,\mathrm{C/m^3}$. This is shown in Fig. 21.

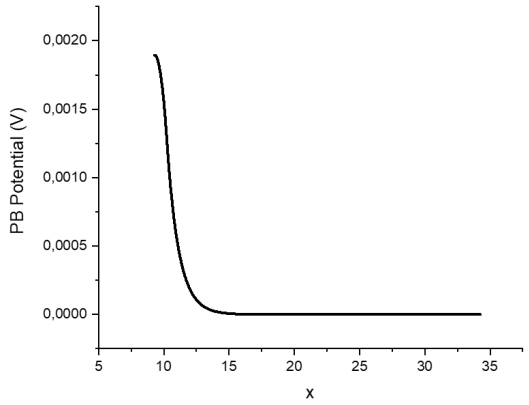

Figure 21: Voltage profile obtained by solving the Poisson-Boltzmann equation for a porous electrode covered by one polyelectrolyte layer of charge density $0.5 \times 10^6\,\mathrm{C/m^3}$ and thickness 2 nm submerged in fresh water.

A much smaller Donnan Potential is obtained, as expected, of 1.8 mV. Let us now add another layer, assuming it will stick much better on it, thus having a bigger thickness and more charge density. It will, however, not be perfect, so we suppose a layer of thickness 11 nm, $\rho_2 = -3 \times 10^6\,\mathrm{C/m^3}$, as shown in Fig. 22.

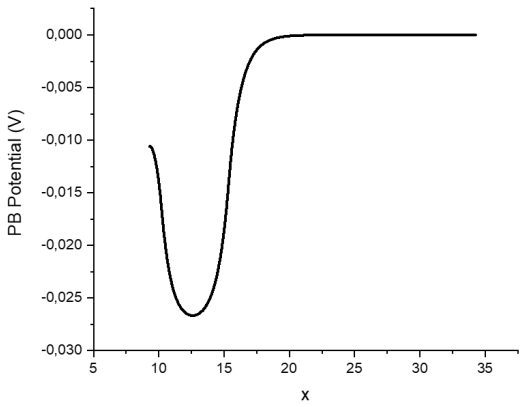

Figure 22: Voltage profile obtained by solving the Poisson-Boltzmann equation for a porous electrode covered by two polyelectrolyte layers, one of charge density $0.5 \times 10^6\,\mathrm{C/m^3}$ and thickness 2 nm, the second one of charge density $-5 \times 10^6\,\mathrm{C/m^3}$ and thickness 11 nm. The electrode is submerged in fresh water.

This time, the Donnan potential yields 10 mV in absolute value, more than five times the result obtained before. We can also simulate the voltage vs surface charge density to study the extracted energy, as shown in Fig. 23. The energy density of one cycle results in $0.028\,\mathrm{mJ/m^2}$.

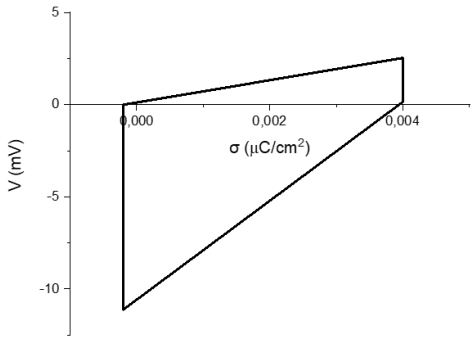

Figure 23: Theoretical voltage vs surface charge density for a carbon electrode. 20 mM and 500 mM waters are exchanged. Polyelectrolyte charge densities of $0.5 \times 10^6\,\mathrm{C/m^3}$ for the first layer, $-5 \times 10^6\,\mathrm{C/m^3}$. Thicknesses of 2 and 11 nm.

5.2.3 Three layers

Finally, let us add a third layer, which would stick to the electrode and the two previous layers even better, and see if it would be possible to improve the previous result. This new layer will have a thickness of 30 nm and a charge density of $15 \times 10^6\,\mathrm{C/m^3}$.

The Donnan Potential is this time somewhat bigger in absolute value, but barely no-

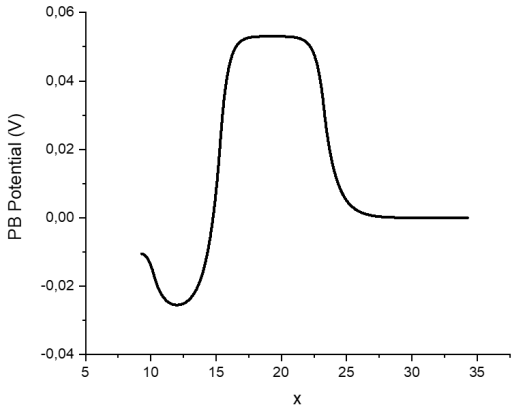

Figure 24: Voltage profile obtained by solving the Poisson-Boltzmann equation for a porous electrode covered by three polyelectrolyte layers. The first one has charge density $0.5 \times 10^6\,\mathrm{C/m^3}$ and thickness 2 nm; the second one, charge density $-5 \times 10^6\,\mathrm{C/m^3}$ and thickness 11 nm; the third one, charge density $15 \times 10^6\,\mathrm{C/m^3}$ and thickness 17 nm. The electrode is submerged in fresh water.

ticeable. This leads us to think that a third layer might not be essential, but this cannot be firmly stated unless proven experimentally. What is clear is it's much smaller influence on the final result, thus a fourth layer is not considered. Because of all this, the graph of voltage vs surface charge density is not shown, being just as the one in Fig. 23 and obtaining the same extracted energy.

6 Experimental results

6.1 Materials and methods

Capmix cell

The capmix cell used in this Bachelor's thesis, developed by Iglesias et al. [29] and explained in [5], is the chamber where the water exchange between electrodes takes place. As it can be seen in Fig. 25 , the cell consists on an acrylic glass cylinder where different elements are located. Both electrodes are placed facing each other on a 2 cm in diameter orifice. Between these, we place a plastic film spacer to prevent the electrodes from touching each other. Inside the cylindrical orifice, between the electrodes, two small wholes allow water to run in and out of the chamber. One face of each electrode is covered by an activated carbon film, while the other one is attached to a copper wire that serves as electric contact.

Potential and current data were recorded at the desired rate in a Keysight 34970A Data Acquisition/Switch Unit (USA). Masterflex™ peristaltic pumps (also connected to the control unit) are used to pump the solutions in the gap between the electrodes. The cell has thus a simple symmetric structure of wire - electrode - film spacer - electrode - wire, all attached to the pipes where the different water solutions run through.

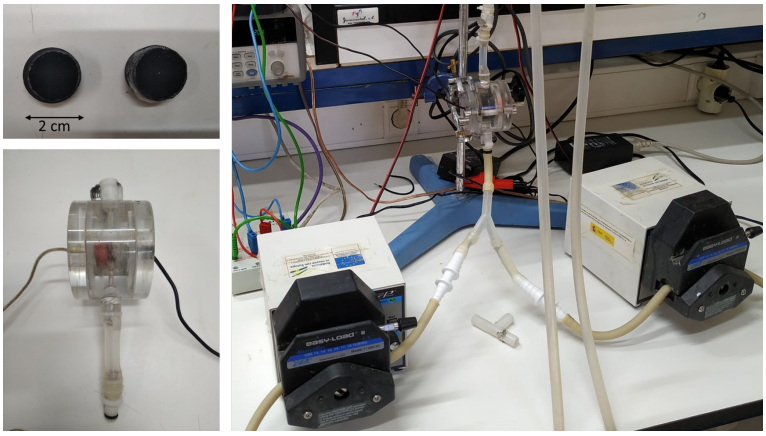

Figure 25: Top left: porous electrodes attached to a graphite cylindrical base. Bottom left: The acrylic glass cell. On the left: the cell attached to the water electrovalves. The left one pumps fresh water, whereas the right one pumps salty water.

Porous electrodes

Two carbon samples were used in the experiments, when possible. One, denominated SR-23, was manufactured by MAST Carbon (UK). Its specific surface area is 927 m^2/g, and its pore size distribution, determined by nitrogen adsorption, indicates predominance of pores below 10 nm and around 80 nm [5]. The other sample, YP80F (Kuraray CO, Japón) has a surface area of 2271 m^2/g, and a highly monodisperse pore size of about 1 nm.

Carbon is an ideal material to build EDL capacitors. The bigger the conductivity, the smaller the leakage will be -one of the main loses source in these capacitors-, and carbon is a material with high conductivity. Furthermore, its unreactivity allows us to work with potentials of the order of 500 mV without the risk of electrochemical reactions. Despite these features, its biggest advantage relies on its enormous surface area, which maximizes charge exchange by allowing more ions to accumulate inside its pores.

The carbon films were made by mixing carbon powder with a binder solution [5]. The solvent used (1-methyl 2-pyrrolidone, NMP) was from Merck (Germany) and the binder, polyvinylidene fluoride (PVDF) from Arkema (USA). The carbon powder is dried in an oven at 105 º for 24 hours. The powder is then mixed with a solution of PVDF and NMP at a concentration of 3 % by weight at 75 ºC while stirring. 90 g are taken from this solution and are mixed with 26.93 g of carbon. The mixture is kept under moderate vacuum conditions. Finally, the electrodes are painted with this solution, aiming to create a very thin layer. This can also be done by aerosol painting, a technique that was not available in our laboratory.

Polyelectrolyte layers

In order to coat the electrodes with anionic/cationic polyelectrolyte layers, the carbon electrodes were submerged inside the corresponding polymeric solutions under magnetic stirring for 72 hours. The electrodes were then rinsed with deionized water and placed inside the cell. The polyelectrolytes used were the following: for the anionic coating, poly (sodium 4-styrenesulfonate) (PSS) with molecular weight 200 000 g/mol. On the other hand, for the cationic coating, the chosen polymer was poly (diallyldimethyl ammonium

chloride) (PDACMAC), with molecular mass 200 000 g/mol [6].

Water solutions

Two water solutions were used, trying to simulate sea and river water. Although sea water contains many compounds ($MgSO_4$, Br, KCl...), only NaCl was considered, being the most relevant one and simplifying the water preparation process. Hence, a 20 mM NaCl solution was used to simulate fresh water and, for salty water, a 500 mM solution [5]. The water used was deionized and filtered in a Milli-Q Academic system from Millipore (USA).

6.1.1 Methods

Two important factors must be considered in the implementation of the capmix method. These are the initial charging conditions and the value of the charging voltage. If done correctly, leakage can be at least partially avoided. There are more factors that contribute to a better experimental design, such as temperature, but they will not be taken into account either because its effect is negligible or because it escapes the main goals of this Bachelor's Thesis.

Charging curves for two CDLE electrodes will be presented, characterizing the different properties of each carbon electrode. Later on, charging cycles for both cells and for different charging voltages will be represented. Finally, experimental results will be shown for one polyelectrolyte layer. No further experiments could be performed due to the quarantine situation that took place while developing this thesis.

6.2 Effect of initial charging conditions

When using high surface area materials for EDL capacitors, high capacitance and energy densities are obtained. However, the disadvantages of these materials must be considered in order to avoid them and improve the overall performance. When a charging process is carried out, the inner elements of the surface of the pores experience little current and, at the same time, the particles that constitute the porous matrix experience high contact resistance [5]. This results in a non-homogeneous charging rate, since it will take a long time for the ions to access the inner parts of the pores. When charging the device, although the current will drop to zero very rapidly, the electrodes will have to remain charging for a much longer period of time to make sure that the ions are fully covering all of the electrode surface. In our case, the results here shown were obtained after a one-night charge where, periodically, fresh and salty water were exchanged.

This phenomenon can be seen as a circuit with three or more capacitors and resistances, where each capacitor will be charged through the resistance sooner than the one below, as can be seen in Fig. 26.

6.3 Applied potential

One could imagine that the higher the surface potential is, the higher the accumulated charge will be. However, there are several limitations to this. In order to avoid electrochemical reactions, for example, all voltages to consider must be smaller than 1 V [30].

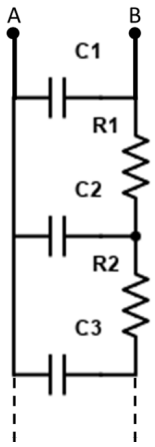

Figure 26: Equivalent circuit of charge redistribution inside a pore.

A very important source of loses (we could actually say the most important one) is leakage. Current leakage appears because of the natural tendency of the voltage difference to move towards a given "spontaneous" potential [31]. Charge will migrate from the electrodes into the solution, thus not all stored charge will be recovered (that is, transferred between electrodes). In a plot of voltage vs. charge, it will be found that successive cycles do not superimpose, as seen in Fig. 27. It has been shown that leakage can be greatly reduced if working with the appropriate charging potential [6], resulting in optimum conditions when the charging voltage is between 350 and 400 mV. For higher potentials, leakage becomes too important and for lower ones energy extraction will never surpass energy input. Charging the cell under the conditions mentioned in the previous section results in a further reduction of leakage. However, it will still be noticeable.

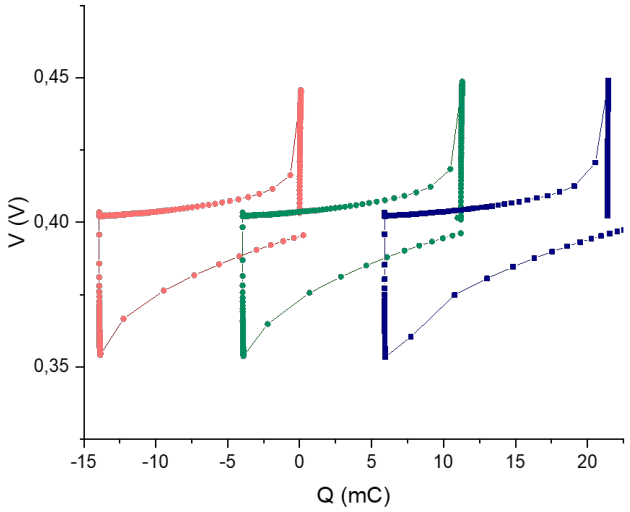

Figure 27: Charge as a function of cell voltage for three consecutive CDLE cycles for SR23 carbon electrodes at a charging voltage of 400 mV.

6.4 Charging curves. Determination of resistance and capacitance of the electrodes

Both sets of electrodes can be characterized considering their capacitance and resistance. We simulate the cell filled with solution as a series RC circuit (where R is the equivalent resistance of the electrodes and the solution between them, and C is the equivalent capacitance of the two electrodes (including their double layers), so that each of them will have a capacitance equal to $2C$. It is hence immediate to find the time dependence of the current when the cell is connected to a voltage source V

$$I(t) = \frac{V}{R}\exp(-t/RC) \tag{6.1}$$

It is then possible to evaluate the charging curve of the cell and obtain its resistance R (at $t = 0$) and capacitance by performing a linear regression in logarithmic scale.

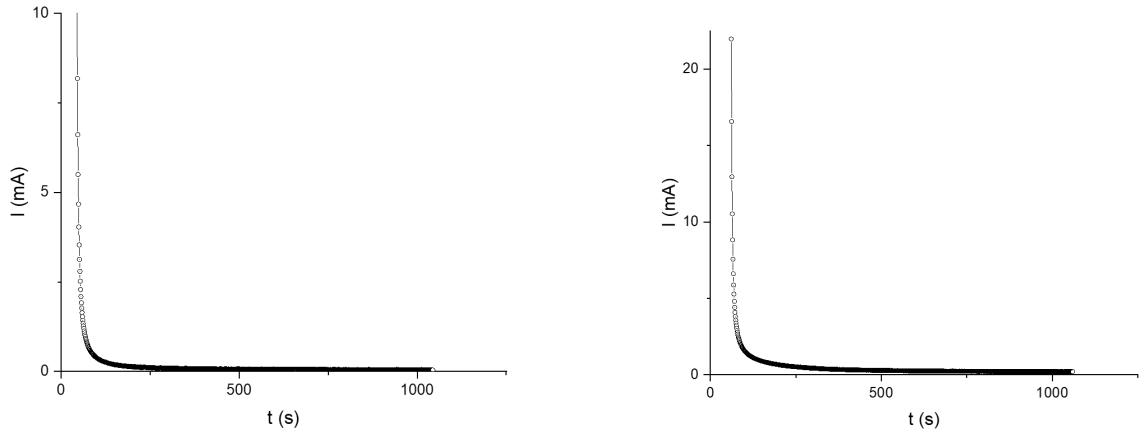

Figure 28: First 1250 s of a charging cycle for SR23 (left) and (YP80F) (right). Applied voltage of $V = 400 \pm 10\,\text{mV}$, salt solution 500 mM NaCl

For the SR23 electrodes, $I(0) = 10.6698 \pm 0.0001\,\text{mA}$, resulting in $R_{\text{SR23}} = 37.5 \pm 0.9\,\Omega$. For the YP80F electrodes, $I(0) = 21.9616 \pm 0.0001\,\text{mA}$, and $R_{\text{YP80F}} = 18.2 \pm 0.5\,\Omega$.

By taking a logarithmic representation, the following equation applies:

$$\ln I(t) = \ln\left(\frac{V}{R}\right) - \frac{t}{RC} \tag{6.2}$$

Hence by studying the slope the capacitance can be obtained. It results in $C_{\text{SR23}} = 34 \pm 3\,\text{mF}$; $C_{\text{YP80F}} = 82 \pm 4\,\text{mF}$. Now what is interesting is not the capacitance itself, but its value per unit of apparent area. Since the electrodes are disks 2 cm in diameter, we obtain:

$$\frac{C_{\text{SR23}}}{S_{\text{SR23}}} = 108 \pm 18\,\text{F/m}^2 \tag{6.3}$$

$$\frac{C_{\text{YP80F}}}{S_{\text{YP80F}}} = 261 \pm 27\,\text{F/m}^2 \tag{6.4}$$

6.5 CDLE Cycles

Fig. 29 illustrates the results obtained with electrodes made of SR-23 carbon particles. Note that the voltage rise is about 50 mV, and that the process is very reproducible. The current is also plotted as a function of time: the charging current peaks at about 3.5 mA, and the discharge one is -2 mA maximum. This is a direct consequence of the larger resistance of the low-NaCl solution. Integrating the product $V{\cdot}I$ with time, the energy balance of each cycle can be obtained. This is represented in Fig. 29b: note that the energy obtained during discharge is lower that that used for charging; leakage is very significant in this sample, and it is suggested that this type of carbon is not suitable for CDLE.

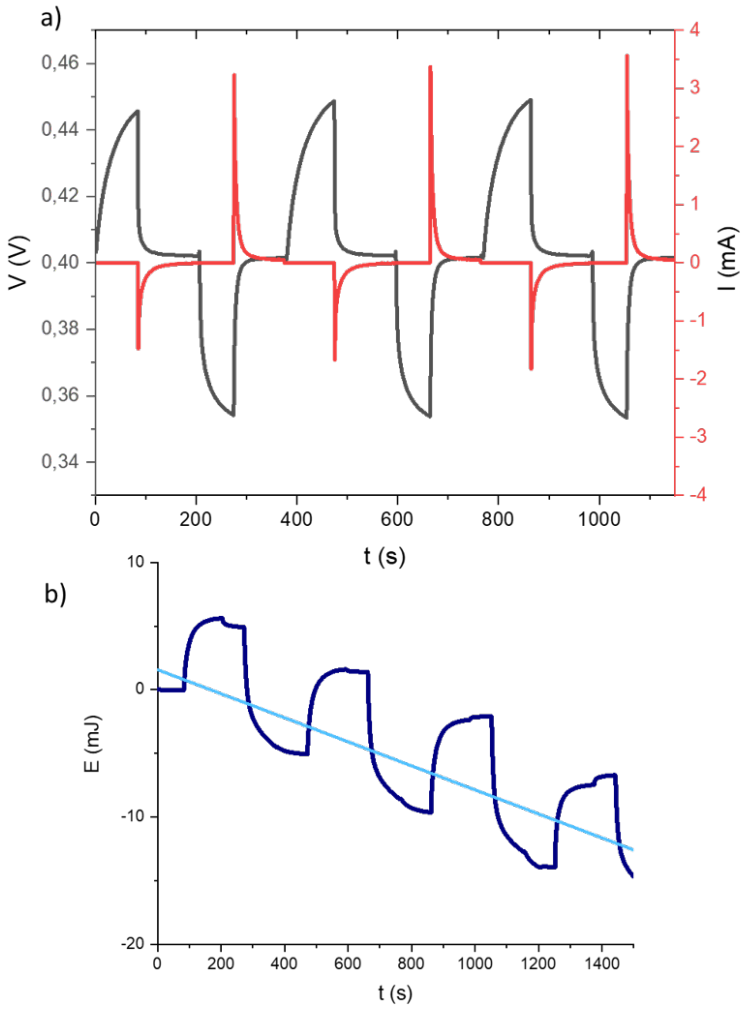

Figure 29: CDLE cycles for SR23 electrodes at a charging potential of 400 mV. a) Voltage and intensity vs. time; b) accumulated energy against time. A linear fitting was used to obtain the average power, given by the linear function's slope.

The resulting power, obtained from a linear fit of energy vs. time is obviously negative: $\bar{P} = -(9.44 \pm 0.05) \times 10^{-3}$ mW. Similar results were obtained for YP80F (Fig. 30), although the power loss is somewhat larger in this case, $\bar{P} = -(3.782 \pm 0.007) \times 10^{-2}$ mW. The value for 300 mV charging potential was $\bar{P} = -(1.817 \pm 0.003) \times 10^{-2}$ mW for

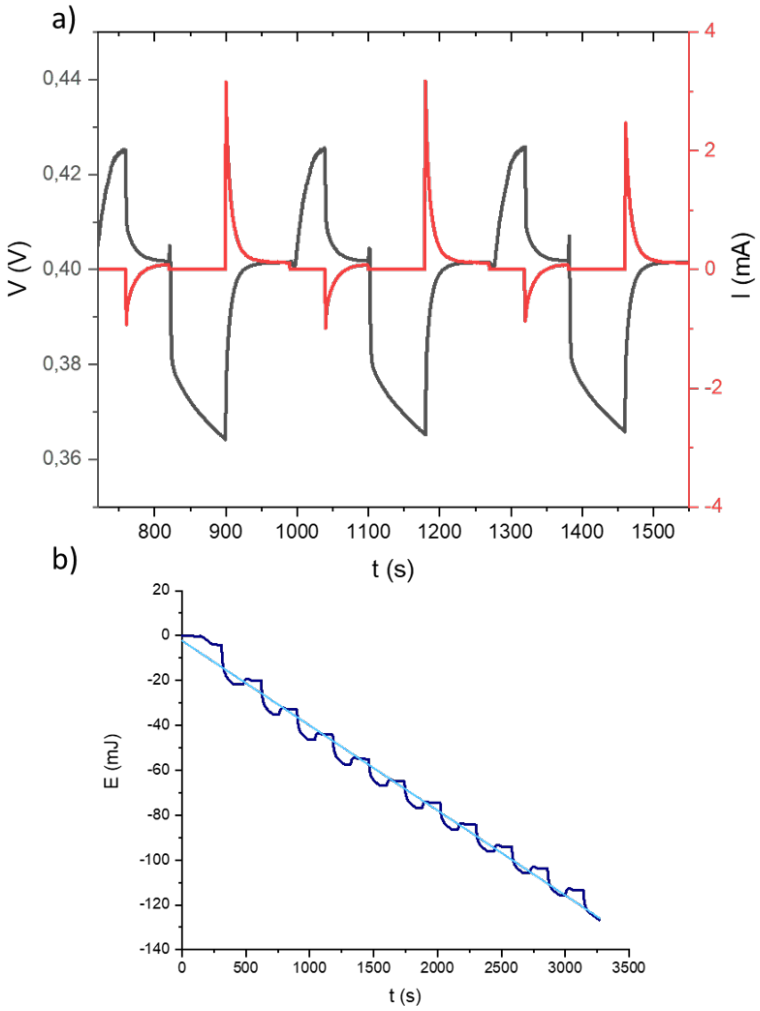

Figure 30: CDLE cycles for YP80F electrodes at a charging potential of 400 mV. a) Voltage and intensity vs time and b) accumulated energy against time. At linear fitting was used to obtain the average power, given by the linear function's slope.

the case of YP80F electrodes and $\bar{P} = -(2.38 \pm 0.10) \times 10^{-3}$ for the SR23 electrodes. Note that in both cases the power losses are indeed smaller in absolute value for the 300 mV charging potential than for the 500 mV potential. This implies that the optimum charging potential must always be studied, since it may depend on the carbon, the shape of the electrode, the thickness of the activated carbon layer etc.

6.6 SE Cycles

These results demonstrate the great improvement that can be reached if a method free of leakage is implemented. As mentioned, SE is a very good candidate for this purpose. A typical cycle was performed as follows (Fig. 31):

- Electrodes are discharged by short-circuiting them.

- The circuit is opened and fresh water is flown through for 110 s. The cell voltage rises to about 60 mV.
- The circuit is closed through a 20 Ω resistance until the cell's voltage returns to zero (100 s).
- Salty water is now allowed in under open circuit conditions for 40 s. The maximum potential is now lower, as expected from the behavior of the Donnan potential.
- Finally, the circuit remains closed, connected to the external load, for 55 seconds. The current now travels in opposite direction, but this is also an energy-productive step.

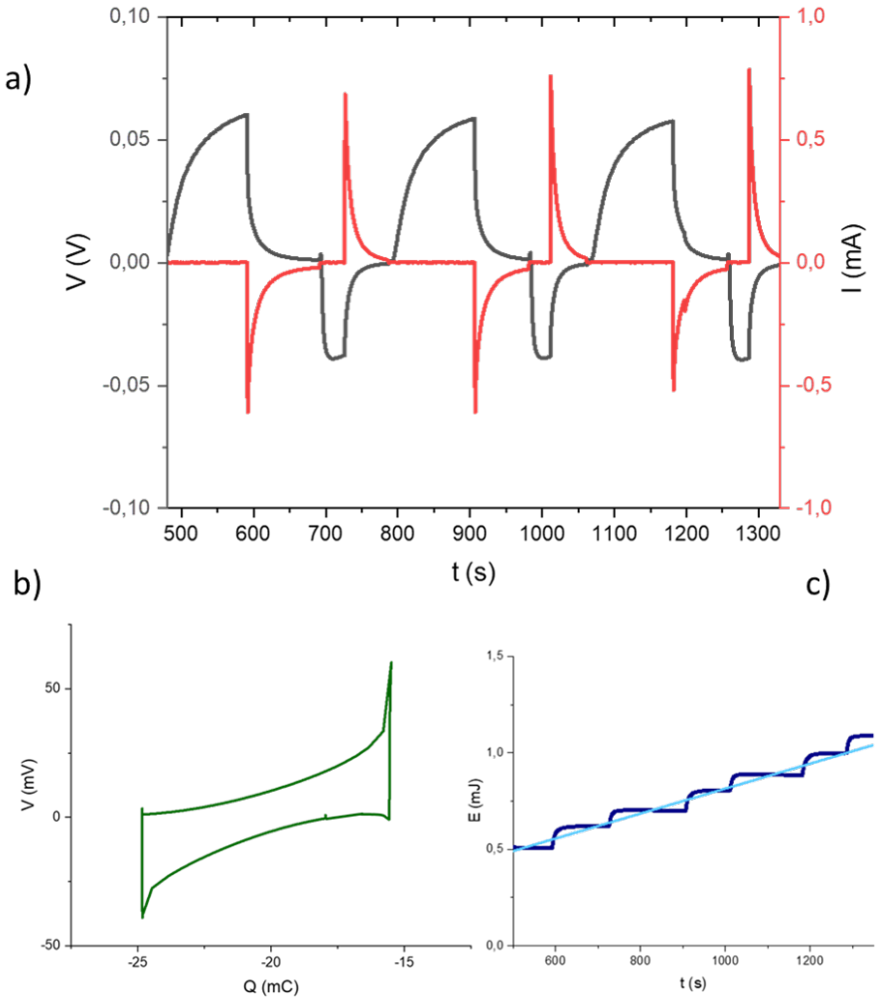

Figure 31: Voltage and current (a) of three consecutive SE cycles for two SR23 electrode coated by antisymmetric polyelectrolyte layers. In (b) potential vs charge for one cycle. In (c) total accumulated energy vs time. In light blue, its linear fit, with its slope being the average power.

The results shown in Fig. 31a can be analyzed using the same methodology as in the CDLE cycles (except that the absolute value of intensity is used at all steps of the cycle). Panel b) shows that the shape of the voltage-charge cycle is as theoretically predicted,

while the integrated energy now **increases** with time, indicating that a positive power is obtained, with average value: $\bar{P} = (6.463 \pm 0.011) \times 10^{-4}\,\mathrm{mW}$, or $2.057 \pm 0.005\,\mathrm{mW/m^2}$ (using the apparent or projected electrode area). In other words, the produced energy is $\bar{E} = (627 \pm 2)\,\mathrm{mJ/m^2}$ per cycle, taking each cycle to last 305 s as commented before. The charge variation, as can be seen in Fig. 31b, is 9 mC, thus the charge density variation is $2.86\,\mathrm{mC/cm^2}$.

We finally observe (see Fig. 9b) that, immediately after closing the circuit, either in salty or fresh solutions, the absolute value of the cell voltage experiences a sudden drop, due to the internal resistance (smaller in the case of higher salt solution) of the cell. When closing the circuit, a voltage $V_R = IR_{salt/fresh}$ appears that is added to the capacitor's voltage difference. Thus we see a drop, corresponding to V_R and later on a typical capacitor discharging curve.

7 Conclusions

In this Bachelor's Thesis we have attempted to improve the modeling and experimental implementation of existing techniques for obtaining clean energy by solution exchanging methods - or blue energy. In order to do this, an extensive understanding of the electrical double layer in porous materials, either raw or coated, appeared necessary. The special conditions on which this Thesis was written under have limited the variety an extension of the results but, despite this, we believe the results are solid enough to be presented and to be a starting point for further improvement. The main conclusions of the work can be summarized as follows:

- We have revised the equations governing the charge and potential profiles around a charged interface. Two situations have been considered: a raw interface, where the solid (conducting) materials are directly put in contact with the solution at work, and one in which a polyelectrolyte layer is interposed between the electrode and the solution (the soft electrode, or SE approach).
- A Matlab routine was written to solve the equations and obtain the charge-potential relationship in all cases.
- The main innovation of this work was to consider that the electrodes are actually coated by two or more layers (of alternatively opposite charge signs, positioned according to the *layer-by-layer* method). The theoretical frame was again resolved and predictions were obtained.
- It was found that the first layer plays a major role in determining the contacting electrode's potential. It has been shown here that two layers can indeed give better results, but this would have to be confirmed experimentally to give more realistic data of the actual thickness of the layers and their charge densities. The control of the properties of the third layer leading to an increase of potential is not so immediate. It is predicted to be often of less significance.
- In any case, the SE technique presents interesting advantages,such as not needing external power sources for charging nor expensive membranes. This leads us to think that it could become a more solid clean energy source in the future.
- The limited experiments that we could carry out demonstrate that is is very difficult to find the conditions in which a raw carbon electrode can produce energy. Charge leakage is a serious drawback that must be carefully faced.
- Experiments with polyelectrolyte coated electrodes (even with a single layer) appear most promising, and our model is able to explain the results even quantitatively regarding the voltage jumps when exchanging solutions.

Summing up, it is clear that deeper research will be needed if one day these techniques are to be developed on an industrial scale. Its advantages are, no doubt, many. There is no need of dynamos or turbines, something that would be very useful for many regions in the world that have no access to electrical power if they live close to a salty water source (around 60 % of the population [32]) and have access to fresh water. The minimum residual wastes, thermal contamination and easy implementation are promising incentives to keep on researching it.

References

[1] R. E. de España", *Avance del Informe del Sistema Eléctrico Español 2019*. Madrid: Red Eléctrica de España, 2019.

[2] T. y. A. D. "Ministerio de Energía, *La energía en España 2016*. Madrid: Ministerio de Energía, Turismo y Agenda Digital. Secretaría General Técnica, 2017.

[3] R. E. Pattle, "Production of electric power by mixing fresh and salt water in the hydroelectric pile," *Nature*, vol. 174, no. 4431, pp. 660–660, 1954.

[4] G. Wick and W. Schmitt, "Prospects for renewable energy from sea," *Marine Technol. Soc. J.*, vol. 11, no. 5-6, pp. 16–21, 1977.

[5] M. Fernández, *Analysis of energy production by salinity exchange in porous electrodes. PhD. Thesis*. Granada: Universidad de Granada, 2017.

[6] S. Ahualli and A. Delgado, *Charge and Energy Storage in Electrical Double Layers*. London: Academic Press/Elsevier, 2018.

[7] R. S. Norman, "Water salination - source of energy," *Science*, vol. 186, no. 4161, pp. 350–352, 1974.

[8] G. L. Wick, "Power from salinity gradients," *Energy*, vol. 3, no. 1, pp. 95 – 100, 1978.

[9] N. Y. Yip, D. Brogioli, H. V. Hamelers, and K. Nijmeijer, "Salinity gradients for sustainable energy: Primer, progress, and prospects," *Environ. Sci. Technol.*, 2016.

[10] R. Pattle, "Production of electric power by mixing fresh and salt water in the hydroelectric pile," *Nature*, vol. 174, no. 4431, pp. 660–660, 1954.

[11] D. Brogioli, "Extracting renewable energy from a salinity difference using a capacitor," *Phys. Rev. Lett.*, vol. 103, p. 058501, July 2009.

[12] B. B. Sales, M. Saakes, J. W. Post, C. J. N. Buisman, P. M. Biesheuvel, and H. V. M. Hamelers, "Direct power production from a water salinity difference in a membrane-modified supercapacitor flow cell," *Environ. Sci. Technol.*, vol. 44, pp. 5661–5665, 2010.

[13] S. Ahualli, M. Jiménez, M. M. Fernández, G. Iglesias, D. Brogioli, and Á. V. Delgado, "Polyelectrolyte-coated carbons used in the generation of blue energy from salinity differences," *Phys. Chem. Chem. Phys.*, vol. 16, no. 46, pp. 25241–25246, 2014.

[14] D. Brogioli, R. Zhao, and P. M. Biesheuvel, "A prototype cell for extracting energy from a water salinity difference by means of double layer expansion in nanoporous carbon electrodes," *Energy Environ. Sci.*, vol. 4, pp. 772–777, Mar. 2011.

[15] D. Brogioli, R. Ziano, R. A. Rica, D. Salerno, O. Kozynchenko, H. V. M. Hamelers, and F. Mantegazza, "Exploiting the spontaneous potential of the electrodes used in the capacitive mixing technique for the extraction of energy from salinity difference," *Energy Environ. Sci.*, vol. 5, pp. 9870–9880, 2012.

[16] O. S. Burheim, F. Liu, B. B. Sales, O. Schaetzle, C. J. N. Buisman, and H. V. M. Hamelers, "Faster time response by the use of wire electrodes in capacitive salinity gradient energy systems," *J. Phys. Chem. C*, vol. 116, pp. 19203–19210, Sept. 2012.

[17] D. Brogioli, R. Ziano, R. Rica, D. Salerno, and F. Mantegazza, "Capacitive mixing for the extraction of energy from salinity differences: Survey of experimental results and electrochemical models," *J. Colloid Interface Sci.*, vol. 407, no. 0, pp. 457 – 466, 2013.

[18] J. Lyklema, "Fundamentals of colloid and interface science," *Vol. II*, 1991.

[19] Á. V. Delgado, *Interfacial electrokinetics and electrophoresis*, vol. 106. CRC Press, 2001.

[20] J. Lyklema, *Fundamentals of interface and colloid science: soft colloids*, vol. 5. Elsevier, 2005.

[21] R. Hunter, *Foundations of Colloid Science*. Oxford: Oxford University Press, 2000.

[22] J. Lyklema, *Fundamentals of Interface and Colloid Science, vol. II: Solid-Liquid Interfaces*. New York: Academic Press, 1995.

[23] H. Ohshima, "A simple algorithm for the calculation of the electric double layer potential distribution in a charged cylindrical narrow pore," *Colloid and Polymer Science*, vol. 294, no. 11, pp. 1871–1875, 2016.

[24] B. B. Sales, F. Liu, O. Schaetzle, C. J. Buisman, and H. V. Hamelers, "Electrochemical characterization of a supercapacitor flow cell for power production from salinity gradients," *Electrochim. Acta*, vol. 86, pp. 298 – 304, 2012.

[25] X. Zhu, W. Yang, M. C. Hatzell, and B. E. Logan, "Energy recovery from solutions with different salinities based on swelling and shrinking of hydrogels," *Environmental science & technology*, vol. 48, no. 12, pp. 7157–7163, 2014.

[26] P. Długołecki, K. Nymeijer, S. Metz, and M. Wessling, "Current status of ion exchange membranes for power generation from salinity gradients," *J. Membr. Sci.*, vol. 319, no. 1, pp. 214–222, 2008.

[27] S. Ahualli, *Propiedades electrocin[U+FFFD]ticas de suspensiones coloidales concentradas*. PhD thesis, University of Granada, 2009.

[28] S. Ahualli, M. L. Jimenez, F. Carrique, and A. V. Delgado, "Ac electrokinetics of concentrated suspensions of soft particles," *Langmuir*, vol. 25, no. 4, pp. 1986–1997, 2009.

[29] G. Iglesias, S. Ahualli, A. Delgado, M. Jimenez, and F. Gonzalez-Caballero, "A device for the measurement of energy by ionic exchange," 2014.

[30] B. Conway, *Electrochemical Supercapacitors: Scientific Fundamentals and Technological Applications*. New York: Plenum Publisher, 1999.

[31] M. Marino, L. Misuri, M. Jiménez, S. Ahualli, O. Kozynchenko, S. Tennison, M. Bryjak, and D. Brogioli, "Modification of the surface of activated carbon electrodes for capacitive mixing energy extraction from salinity differences," *J. Colloid Interface Sci.*, vol. 436, no. 0, pp. 146 – 153, 2014.

[32] J. E. Cohen, C. Small, A. Mellinger, J. Gallup, and J. Sachs, "Estimates of coastal populations," *Science*, vol. 278, no. 5341, pp. 1209–1213, 1997.